Elucidation of the Mechanistic Aspects of Chemical EOR in Viscous Oil Systems

Danial Arab [a, b, c, d, e], **Steven L. Bryant**[b], **Ole Torsæter**[c], **Peter Englezos** [d], **Bhushan Gopaluni** [d], **Apostolos Kantzas**[b, e]

[a] DarkVision Technologies Inc., 111 Forester St, North Vancouver, BC, CANADA, V7H 0A6

[b] Department of Chemical and Petroleum Engineering, University of Calgary, 2500 University Drive NW, Calgary, AB, CANADA, T2N 1N4

[c] PoreLab Center of Excellence, Department of Geoscience and Petroleum, Norwegian University of Science and Technology (NTNU), N-7491 Trondheim, Norway

[d] Department of Chemical and Biological Engineering, The University of British Columbia, 2360 East Mall, Vancouver, BC, CANADA, V6T 1Z3

[e] PERM Inc., 2221 41 Ave NE, Calgary, AB, CANADA, T2E 6P2

E-mail addresses:

danial.arab@darkvisiontech.com

steven.bryant@ucalgary.ca

ole.torsater@ntnu.no

peter.englezos@ubc.ca

bhushan.gopaluni@ubc.ca

akantzas@ucalgary.ca

Contents

Abstract

Chemical enhanced oil recovery techniques have been suggested as efficient alternatives to thermal methods in many thin/small viscous oil reservoirs in western Canada. These acidic oil reservoirs have been screened as good candidates for alkaline (A) and surfactant (S) floods. In this study, sand-pack core flooding experiments and pore-scale microfluidic tests were designed to give some new insights on the mechanisms of AS floods augmented with polymer (P) solutions in viscous oil systems.

Viscous oil samples from Luseland field (14,850 mPa.s at 25 °C) was used in all the experiments. The most efficient chemical generates ultralow interfacial tension, 0.002 mN/m, producing low viscosity type II (+) emulsion (740 mPa.s, which is much lower than the viscosity of originating oil). The two pore volumes injection of this cocktail results in around 20 % OOIP incremental oil recovery, which is almost doubled after injecting two pore volumes of extended water. The core effluents were all low viscosity oil in water emulsions, consistent with observations in batch mixing experiments. The incremental oil recovery to ASP flood is almost twice the recovery obtained in the polymer flood with nearly 4.5 times larger pressure build-up across the core. These observations suggest that the main mechanism is emulsification and oil entrainment rather than improvement in sweep efficiency.

These speculated mechanisms based on the core scale observations were verified through the results of the microfluidic experiments. ASP solution can efficiently penetrate the residual ganglia or the edge of the water channels from which oil can be efficiently stripped. This oil is easily entrained in the form of low viscosity oil in water emulsions. Our results emphasize the critical role of polymer in the cocktail. In the absence of polymer, AS cannot efficiently penetrate the residual viscous oil leading to only a minuscule improvement in oil recovery.

Introduction

Oil recovery to primary solution gas drive in unconventional Canadian viscous oil reservoirs, with oil viscosities up to 50,000 mPa.s, is estimated as low as 5 % original oil in place (OOIP), which can be almost doubled when it is supplemented with water flooding. This leaves around 90 % OOIP residual oil at the end of water flooding as a huge target for enhanced oil recovery (EOR) processes. This residual oil is continuous in the regions where water did not invade due to severe viscous fingering. Thermal EOR processes have been reported to be inefficient in

thin/small/shallow Canadian viscous oil reservoirs or when there are top or bottom water zones (Zhou *et al.*, 2016). In these reservoirs, unfavorable mobility ratio and the resultant viscous fingering make the solvent-based EOR techniques uneconomical, where injection of a lot of solvent is required to sufficiently pressurize the reservoir (Rangriz Shokri and Babadagli, 2016). These challenges make thermal and solvent-based EOR techniques cost-ineffective (Dong *et al*., 2011). Therefore, chemical EOR processes have gained considerable attention to recover residual oil in viscous oil reservoirs.

In chemical EOR techniques, a chemical formulation (surfactant (S), alkaline (A), alkaline-surfactant (AS), or the combination of each with a polymer (P) solution) is injected into the reservoir to enhance microscopic displacement efficiency through IFT reduction or increase macroscopic/sweep displacement efficiency through dampening viscous fingering (Bryan and Kantzas, 2007; Sim *et al*., 2014). Viscous oil reservoirs in Western Canada possess high acidic components (TAN > 0.5 mg KOH/g, Dong *et al.*, 2011). Injected alkaline can react with the naphthenic acids in crude oil to create in-situ soap (Liu *et al*., 2010), enhancing viscous oil emulsification (Farouq Ali, 2006). Precise emulsion screening experiments are required to find the desired emulsion type. It is also reported that adding alkaline to the synthetic surfactant preconditions the reservoir rock through increasing its negative charge density (Manrique *et al.*, 2007), which in turn reduces adsorption/loss of synthetic surfactant (Hirasaki *et al.*, 2008). Various studies have been done to investigate the chemical EOR processes, which can be categorized into three main phases: batch (phase behavior) mixing experiments to screen the optimal chemical formulation, core flooding experiments to indirectly investigate/quantify the effect of the selected formulation to displace oil in place while flowing through the pore space, and microfluidic experiments to directly visualize/confirm the mechanisms speculated in the core flooding experiments. In the following, the pertinent literature discussing each phase of the chemical EOR processes is reviewed.

Background

Screening experiments

Screening experiments were first introduced by Stegemeier (Nelson *et al*., 1984) to map the activity of a chemical formulation. This approach consists of batch mixing experiments to determine the active region where ultralow interfacial tension is attained to create low viscosity

microemulsion (Nelson *et al*., 1984). With increasing salinity, expressed as total sodium ion concentration in the aqueous phase (Nelson *et al*., 1984), there may be Winsor type I, also called under-optimum (bottom-phase oil in water emulsion), Winsor type II (upper-phase water in oil emulsion), or Winsor type III also called near-optimal (middle-phase low viscosity microemulsion, positioned between the upper oil phase and bottom aqueous phase) (Liu *et al*., 2010). What governs the formation of each emulsion type is a gradient in soap/surfactant ratio (Liu *et al*., 2010), which can be identified through batch mixing experiments where synthetic surfactant concentration keeps constant while alkaline concentration is systematically changed. Nelson and Pope (Nelson and Pope, 1987) revisited the Winsor definitions and identified type II (+), which only contains two phases (upper low viscosity microemulsion and lower aqueous phase). Phase behavior studies are aimed to identify Nelson and Pope type II (+) or Winsor type III emulsions, which are reported as the most efficient states to favorably produce residual oil trapped by capillary forces. However, some studies also reported an advanced effect of high viscosity water in oil emulsion (Winsor type II) to improve sweep efficiency and produce the continuous residual oil left behind in bypassed areas (Aminzadeh *et al*., 2016). In this regard, Liu *et al.* (Liu *et al*., 2010) also commented that the similar ultimate oil recovery may be attained through injecting an ASP formulation generating Winsor type II emulsion compared to injecting a formulation generating Winsor type III emulsions. However, the much larger ASP slug size is required in this case. This may implicitly indicate that improving oil recovery through IFT reduction and producing capillary trapped residual oil is more pronounced compared to the improving sweep attained through generating high viscosity water in oil Winsor type II emulsions.

Core flooding experiments

Table 1 summarizes literature discussing chemical EOR processes in viscous oil systems at the core and pore levels. Bryan and Kantzas (Bryan and Kantzas, 2008) reported that AS flood results in the in-situ formation of emulsions in the preformed water channels, which in turn can efficiently block them off. In this case, relative permeability to the aqueous phase is reduced, which leads to 6.8 to 18.0 % incremental heavy oil (oil samples from a field in Saskatchewan with a viscosity of 11,500 mPa.s at ambient temperature) recovery in various runs (Bryan and Kantzas, 2008). They relied on low field NMR and pressure response observed in the sand-pack flood experiments to indirectly determine the emulsion types. They reported the possibility of formation of water in oil emulsions even in deionized AS system. They commented that this inference could partially

explain the observed incremental oil recovery, which requires more direct investigation through pore-scale investigation. In another study, Liu *et al*. (Liu *et al*., 2007) reported that the formation of oil in water emulsions and oil bank are necessary for the AS -assisted incremental oil recovery. They provided microscopic images of oil in water emulsion from the bottle tests and extended this observation to the emulsion formation during flow in porous media. On the other hand, the observed pressure drop was dramatically large which favors formation of water in oil emulsions. They did not comment on this contradiction. In another study, Dong *et al*. (Dong *et al*., 2009) reported 22-23 % OOIP incremental viscous oil from the Brintnell reservoir (Alberta, Canada) recovery due to the formation of oil in water emulsions. This study also used bottle tests to determine the emulsion type. Kumar *et al.* (Kumar *et al.*, 2012) used hydrophilic surfactant along with Na_2CO_3 to ensure the formation of viscous crude oil, 10,000 mPa.s at room temperature, in water emulsions with viscosities smaller than that of the originating oil. They reported 10 to 35 % OOIP due to injection of the chemical cocktail into the sand-pack. In a more recent study, Aminzadeh *et al.* (Aminzadeh *et al.*, 2016) conducted some flooding experiments using both consolidated and unconsolidated sand packs to investigate the effect of different surfactants along with alkaline to enhance oil, crude samples from a field in South America with a viscosity of 350 mPa.s, recovery. They reported improvement in sweep efficiency due to the formation of high viscosity water in oil emulsion as the dominant responsible rather than oil entrainment for the observed 29 to 34 % OOIP incremental oil recovery. They claimed that the alkaline could react with the crude to generate hydrophobic soap, leading to water formation in oil emulsion.

Table 1: Summary of literature discussing mechanisms of chemical EOR processes in viscous oil systems at core (core flooding experiments) and pore (microfluidic experiments) scales

Core flooding experiments					
Oil viscosity (mPa.s)	Core type	Core characteristics		Chemical formulation	Reference
		K (d)	ϕ (%)		
1,800	Sand-pack	2.5 to 3	35.4 to 37.2	NaOH and Na_2CO_3 and anionic	Liu *et al.*, 2007

				surfactant (alkyl ether sulfate)	
11,500	Sand-pack	0.7 to 19.2	41 - 49	Anionic surfactant and Na_2CO_3	Bryan and Kantzas, 2008
1,266	Sand-pack	2.5 to 3.5	36	Anionic surfactant and NaOH and Na_2CO_3	Dong *et al.*, 2009
10,000	Sand-pack	20 to 30	35 to 44	hydrophilic surfactant and Na_2CO_3	Kumar *et al.*, 2012
350	Consolidated and unconsolidated sand-packs	23 - 35	2 - 7	Alkaline along with seven different surfactants	Aminzadeh *et al.*, 2016
Microfluidic experiments					
Oil viscosity (mPa.s)	Microfluidic chip pattern	Microfluidic chip characteristics		Chemical formulation	Reference
		K (d)	ϕ (%)		
562[a]	A single channel with pore body depth, length, and width of 20, 1400, and 400 µm, respectively	N/M[b]	N/M[b]	Na_2CO_3 and Commercial polymer HPAM	Su *et al.*, 2022

470, 1,773, 7,146[c]	A chip consists of two layers: high permeability with average pore size of 60 µm and low permeability layers with average pore size of 30 µm	N/M[b]	47	Anionic, cationic, and non-ionic surfactants	Hu *et al*., 2022
1,202[d]	N/M[b]	N/M[b]	N/M[b]	NaOH and Na_2CO_3	Gong *et al*., 2016
43	Periodic random pore geometries with hexagon, square, diamond, and triangle-shaped matrix	~ 0.2	~ 19	Surfactant (NEODOL 91-8 ethoxylated alcohol)	Xu *et al*., 2014
68	Homogenous with fractures of various orientations	1.6 - 2	52.3	Combinations of various alkali (NaOH, Na_2CO_3, KOH), polymers (hydrolyzed and non-hydrolyzed polyacrylamide, xanthan biopolymer) and surfactants (CTAB and SDS)	Sedaghat *et al*., 2016

1,673[e]	Heterogenous network of interconnected channels and pores with average size of 100 μm	N/M[b]	N/M[b]	Surfactant (Tween 20)	Bazazi *et al*., 2019
10, 86, 505	N/M[b]	N/M[b]	N/M[b]	Only water flooding was conducted	Mei *et al*., 2012
751	2-D Hele-Shaw Cell	N/M[b]	N/M[b]	Non-ionic surfactant, anionic polyacrylamide	Guerrero *et al*., 2018

[a] reported at 65 ˚C

[b] N/M: Not mentioned

[c] reported at 60 ˚C

[d] reported at 22 ˚C

[e] The initial bitumen viscosity was 93,114 mPas. The bitumen was diluted with Heptane (10:1 wt. ratio) to be able to perform microfluidic experiments at room temperature.

Microfluidic experiments

lab-on-a-chip micro-technology has been extensively used in various research areas such as material engineering to formulate emulsions with a precise and controllable droplet size (Schroen *et al*., 2015; Holtze, 2013; Tong *et al*., 2017; Xu *et al*., 2006), food engineering to detect microbes in food and under particular environmental conditions (Neethirajan *et al*., 2011; Weng and Neethirajan, 2017), renewable energy engineering and fuel cells (Banerjee *et al*., 2019; Kjeang *et al*., 2009), reservoir engineering to investigate fluid flow in porous media and understanding the mechanisms suggested for various enhanced oil recovery (EOR) techniques (Afrapoli *et al*., 2012; Ott *et al*., 2019; Li *et al*., 2018), biomedical engineering to conduct diagnostic studies (Sackmann *et al*., 2014), spatial and temporal control of cell growth (El-Ali *et al*., 2006), DNA amplification (Zhang and Ozdemir, 2009), developing novel drug delivery systems (Zhao, 2013; Dittrich and

Manz, 2006; Riahi *et al*., 2015) etc. Micromodels' application in petroleum reservoir engineering dated back to 1952 when Chatenever and Calhoun (Chatenever and Calhoun, 1952) presented one of the earliest publications to study microscopic mechanisms of fluid flow in porous media. They used a flow cell consisting of two plates between which was filled with a single layer of matrices made of either water-wet glass or oil-wet Lucite spheres.

Various techniques such as Hele-Shaw, glass beads, different types of lithography (optical, stereo, and soft), and various types of etching (wet, dry, and laser or plasma) have been developed to fabricate micromodels of different materials, which is reviewed by Karadimitriou and Hassanizadeh (Karadimitriou and Hassanizadeh, 2011). In addition, generating various patterns have been advanced from simple and regular geometry in the early models (Chatenever and Calhoun, 1952) to more sophisticated geometries. Topology of the porous medium in nowadays micromodels can be classifies as perfectly regular, partially regular, fractal, and irregular patterns (Karadimitriou and Hassanizadeh, 2011). These patterns are varied based on the placement of pores within the network based on the various statistical distribution of pore bodies and throats of various sizes determining pore network porosity and permeability (Tsakiroglou and Avraam, 2002; Sbragaglia *et al*., 2007, and Chen and Wilkinson, 1985). Visualization of different patterns of fluid flow in porous medium is the main purpose to use micromodels in reservoir engineering domain. Therefore, transparent materials such as glass, silicon (Kumlangdudsana *et al*., 2007), polydimethylsiloxane (PDMS) (Kunstmann-Olsen *et al*., 2012), and polymethylmethacrylate (PMMA) (Liu *et al*., 2009) have been applied to make micromodels. Detailed review on various fabrication techniques and pros and cons of different materials have been presented by Karadimitriou and Hassanizadeh (Karadimitriou and Hassanizadeh, 2011). In addition to the advantage of micromodels to visualize fluid flow phenomenon at pore scale, they are mainly 2-D which is more realistic compared to 1-D core flooding experiments in reservoir engineering domain. 3-D microfluidic devices have been also designed to study spatial three-dimensional liquid chromatography (Wouters *et al*., 2014). Xu et al., (Xu *et al*., 2017) also presented a technique to create a 2.5-D micromodel, where cross-sections of channels are strictly rectangular rather than being trapezoidal as is in 2-D models. They claimed that their technique improves HF etching technique which generates non-ideal cross-sections. Investigation of the details on fabrication of 3-D microfluidics is not the main concern of this manuscript and reader is referred to Lifton, 2016 and Anbari *et al*., 2018 among others for further details.

In light oil domains, microfluidic chips have been extensively used to understand the interactions between a chemical formulation and oil in place with viscosities below 30 mPa.s (Seo *et al*., 2018; Mejia *et al*., 2019). Conducting microfluidic experiments in viscous oil systems, however, is much more challenging. Table 1 summarizes the literature discussing application of microfluidic chips in viscous oil systems. As shown in Table 1, oil viscosities are mostly below 1,000 mPa.s unless either the experiment was conducted at high temperature or viscous oil was diluted. In this study, however, both sand-pack core flooding and microfluidic experiments were designed to study the efficiency of the chemical formulation to displace Canadian viscous oil (with viscosity of around 15,000 mPa.s at room temperature). Both phase behavior and interfacial tension measurements were applied to identify the best chemical formulation. Supplementary viscosity measurements and emulsion droplet size analysis were conducted to verify the effect of the chemical formulation as viscous oil emulsifier.

Materials and methods

Fluids and screening experiments

Luseland heavy oil samples (14,850 mPa.s and 980 kg/m3 at 25 °C, total acid number (TAN) of 1.72 mg KOH/g, and asphaltenes content of 14.6 wt. %) were used in all the experiments (screening experiments, sand-pack core flooding, and microfluidic experiments). Based on our previous screening experiments (Arab *et al*., 2018), anionic surfactant (sodium alkane sulfonate) and sodium carbonate (Na_2CO_3) were selected as efficient chemicals to emulsify Luseland viscous oil. The spinning drop technique (KRÜSS Spinning Drop Tensiometer) was used to measure interfacial tension (IFT). A Brookfield viscometer (HBDV-II Plus) was used to measure viscosity. A high molecular weight polyacrylamide (FLOPAM^{TM} EM 640 CT, from SNF company) was used as the polymer, which were extensively used for high permeability, viscous oil reservoirs. The polymer solution was filtered three times using a membrane to make sure that the homogenous solution is used in all the experiment. In all the experiments, deionized water (DIW) was used as the base fluid in which different chemicals were dispersed.

Sand-pack core flooding experiments

In all the sand-pack core flooding experiments, uniform silica sands (50 – 70 mesh) were used to prepare the sand-packs of 30.70 cm long with internal diameter of 1.57 cm. DIW was used to saturate the packed bed, which was pre-vacuumed for 30 min. The bed was weighed before and after saturation step allowing calculation of bed porosity. Darcy's law was applied to measure bed

permeability to water: water was injected at various flow rates while measuring pressure drop across the sand-pack. The sand-packs porosity and permeability were in the range of 37.15 ± 0.18 % and 38.79 ± 1.85 Darcy, respectively. All the chemical flooding experiments were done in a tertiary mode i.e., the core at the initial condition (10% connate water saturation) was water flooded for 7 pore volumes of injected (PVI), followed by 2 PVI chemical flood, followed by 4 PVI extended water flood. In all the flooding steps, injection velocity was chosen as 0.7 ft/d (2.5×10^{-6} m/s) to be field representative. The schematic of core-flooding experimental set-up is depicted in Fig. 1.

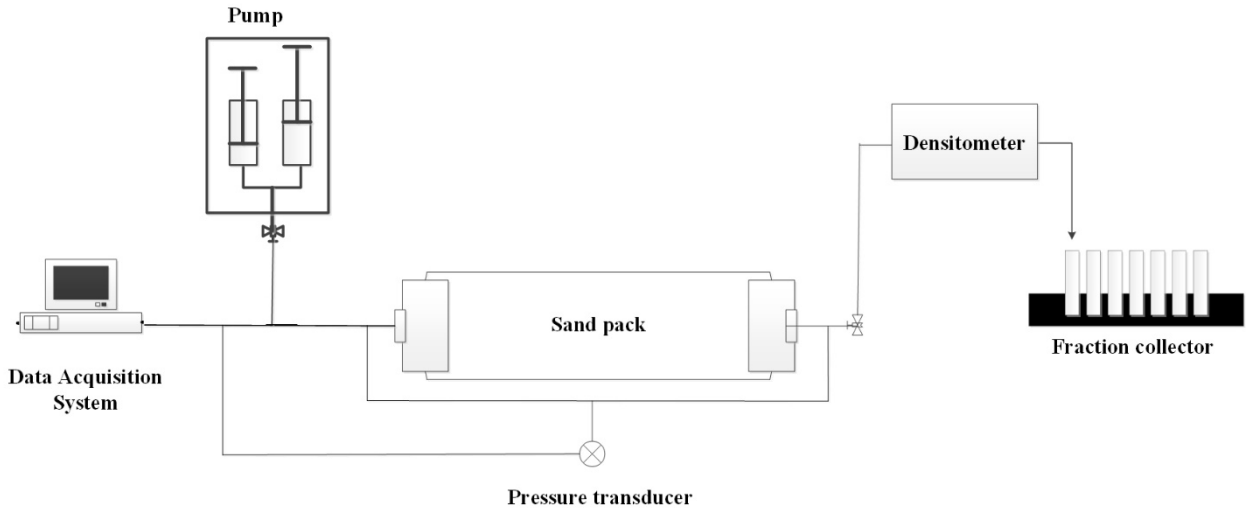

Fig. 1: Schematic of the sand-pack flooding apparatus (Arab *et al*., 2020)

Microfluidic experiments

Experimental procedure

Borosilicate microfluidic chips, from Micronit microtechnology, with dimensions of 45 × 15 × 1.8 mm and a physical rock network, depicted in the image enclosed in Fig. 2, were used in all the experiments. The pattern is generated through random placement of rock-shaped structures, obtained through accurate cutting of rock samples, on the chip (Micronit Microtechnology Product Document). Homogenous etching depth of 20 μm was applied to create the chips' 2D porous medium with dimensions of 20 × 10 × 0.02 mm (Ott *et al*., 2019). Eight capillaries were placed in each side of the chip acting as distributors to assure uniform fluid movement in both injection and production sides. As shown in Fig. 2, a syringe pump was used to inject fluids into the microfluidic chip, which was placed under the microscope equipped with a digital camera to capture images

during flooding. The porosity, permeability, and pore volume of the microfluidic chips are 57 %, 2.5 D, and 2.3 µL, respectively.

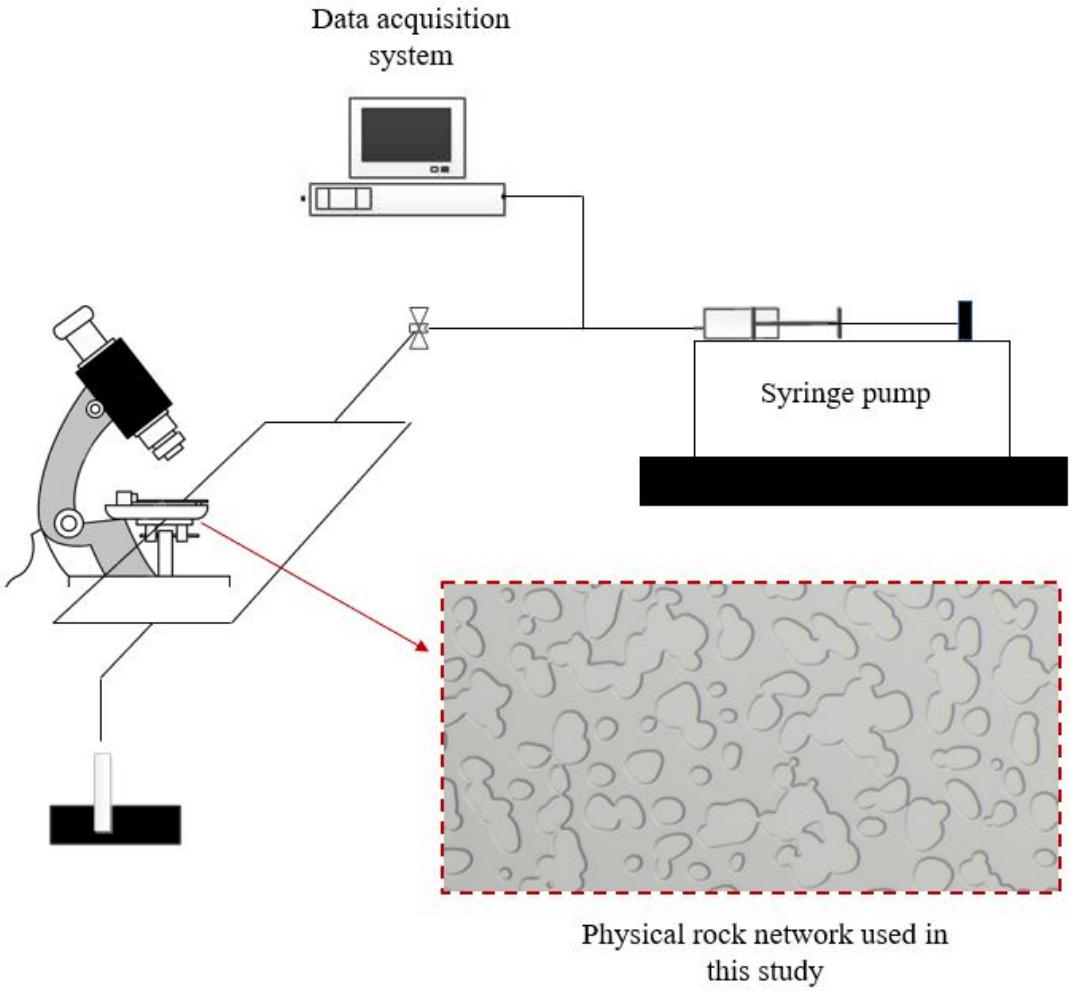

Fig. 2: Schematic of microfluidic apparatus (Arab *et al*., 2021)

Microfluidic chip was vacuumed for 2 hrs before being fully saturated with DIW. Afterwards, heavy oil was injected to displace water in place and reaching connate water saturation. After this oil flooding step, all the capillaries in both injection and production sides were filled with heavy oil. Next, water was injected to displace heavy oil in place. However, due to build-up of too much pressure in capillaries in the injection side of the chip the line was detached making the water flooding step impossible. This could be the main reason for lack of studies on the application of microfluidic chips in heavy oil domain. To overcome this challenge, the experimental protocol was modified: first the chip was fully saturated with DIW (Fig. 3a), then heavy oil was injected in

a reversed direction from right to left (Fig. 3b). Fig. 3c shows how heavy oil front advances from right to left to displace DIW. To assure heavy oil does not enter the left side capillaries, oil injection was stopped at the moment heavy oil reached the end of porous medium (Fig. 3d). The final state of the analyzing window prior to water flooding is shown in Fig. 3e. Afterwards, water was injected from left side whose capillaries are filled with DIW to displace heavy oil in place. This technique allows successful implementation of water flooding to displace heavy oil. In these experiments, the same flooding protocol as applied in the sand-pack core flooding experiments was applied. The chip at irreducible water saturation was water flooded for 5 PVI. Then the chip was flooded with ASP, AS, and P solutions in three different runs. Finally, each experiment was concluded with extended water injection. Injection velocity in all the runs were the same as velocity applied in the sand-pack core flooding experiment i.e., 0.7 ft/d (2.5×10^{-6} m/s). In the end, water injection velocity in the extended water flood was increased from 0.7 ft/d (2.5×10^{-6} m/s) to 24.3 ft/d (8.57×10^{-5} m/s) to investigate the effect of increasing viscous forces to displace residual ganglia.

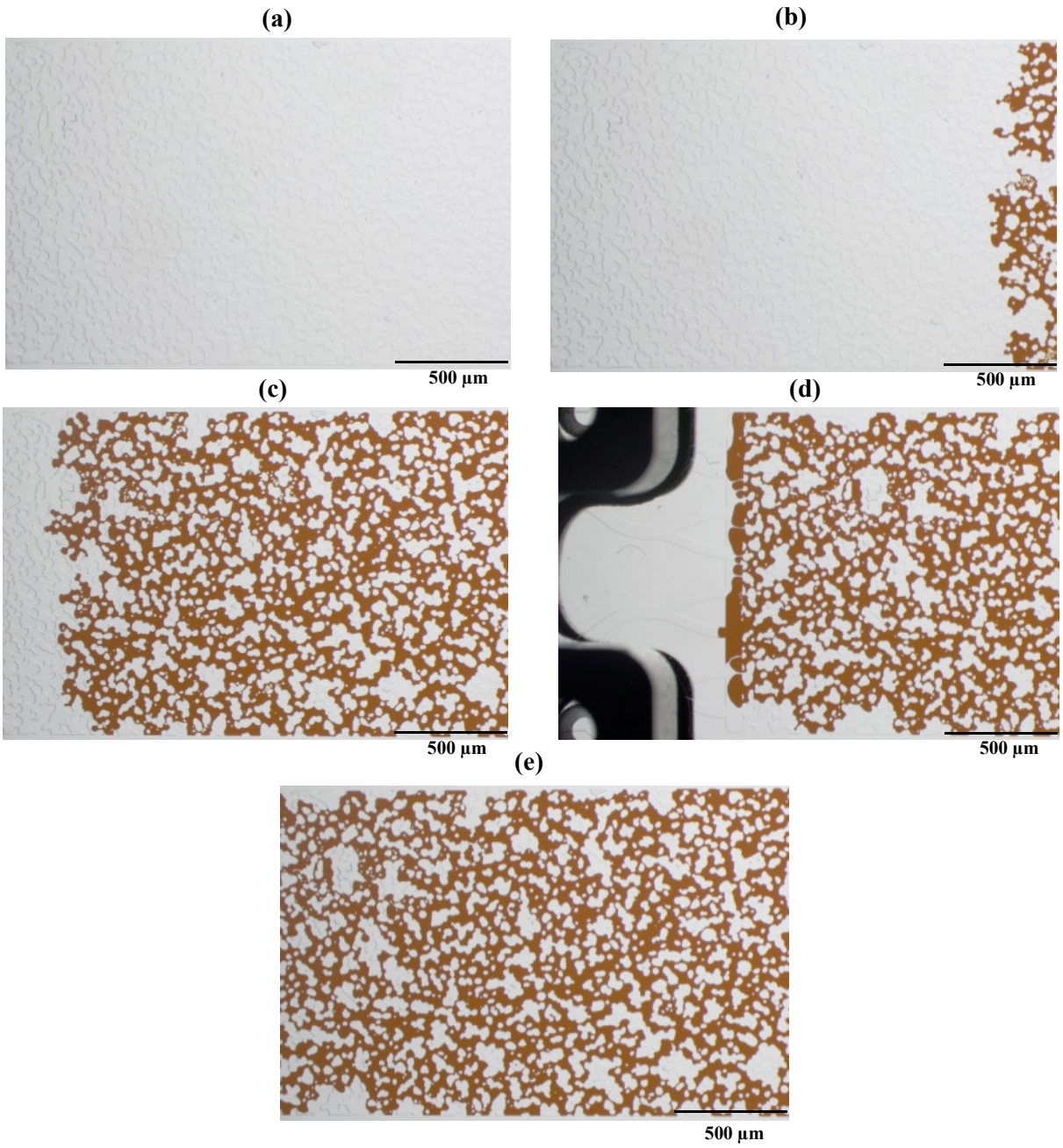

Fig. 3: Microfluidic chip experimental procedure: a) chip was fully saturated with deionized water b) heavy oil was injected from right to left, c) heavy oil uniformly displaces DIW d) heavy oil injection was stopped to assure oil does not enter the capillaries e) final fluid distribution in the analyzing window before starting water flood

Image analysis procedure

The analyzing window (16 × 10 mm) was chosen to safely exclude the capillary end effects. The captured images were segmented to study the effect of various chemicals. Random forest classifier was used as the traditional supervised machine learning algorithm to perform pixel

level image segmentation. Ground truths were generated using an annotation platform, apeer.com (Fig. 4b). As shown in Fig. 4c, oil, water, and glass were labelled as white, black, and gray, respectively. The training dataset containing a feature bank along with the ground truth masks were used to train the Random Forest classifier, which was then used to segment the images not being used to train the model. The feature bank was framed using original pixel values, Gabor kernels (OpenCV (Open-Source Computer Vision Library) documentation on Gabor kernels), various edge detection kernels (Canny, Roberts, Sobel, Scharr, and Prewitt), Gaussian, Median, and Variance kernels. Formulating the Random Forest classifier with the features bank allows us to precisely segment each pixel, which in turn was used to quantify the effect of various chemicals on oil recovery. All the scripts were generated in Python using OpenCV.

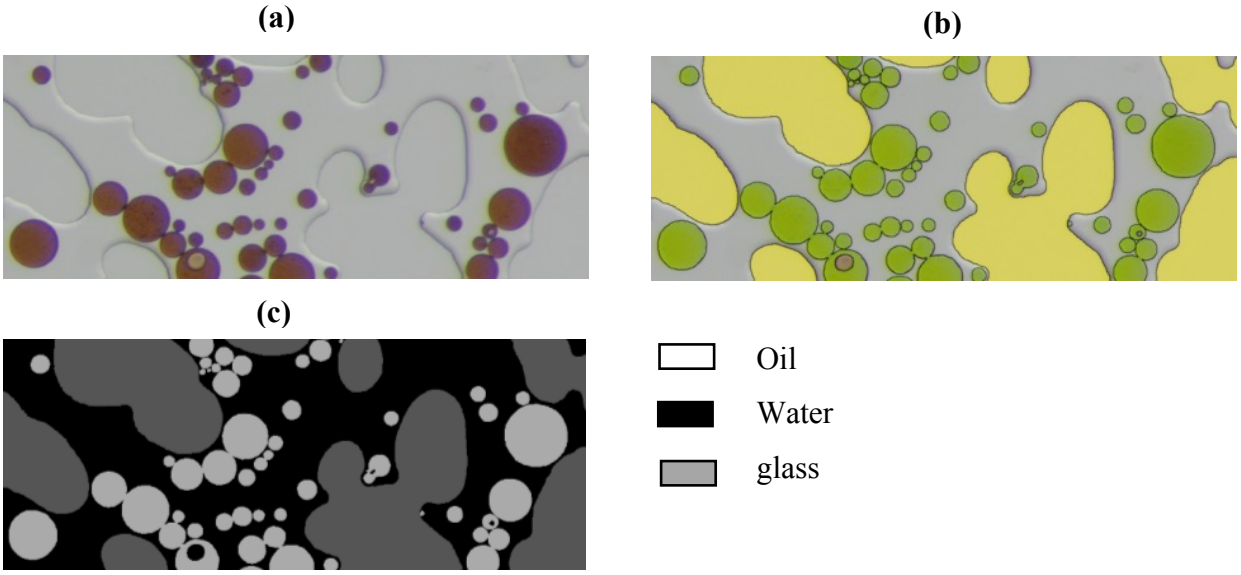

Fig. 4: A close-up view of microfluidic chip images: a) the raw image captured during the experiment, b) the corresponding annotated image used to generate ground truth, c) ground truth used as training dataset to train Random Forest classifier

Results and discussion

Screening experiments

Batch mixing experiments

In the batch experiments surfactant and polymer concentrations were kept constant (0.1 wt. %) while alkaline (Na_2CO_3) concentration was increased from 0.1 to 0.5 wt. % (from leftmost to the rightmost vial in Fig. 5). In these experiments water oil ratio was kept constant and equal to 4 to 1. The vials were gently rotated for 24 hours and then left to reach equilibrium. Fig. 5a and b depicts the vials before mixing and 24 days after rotating, respectively.

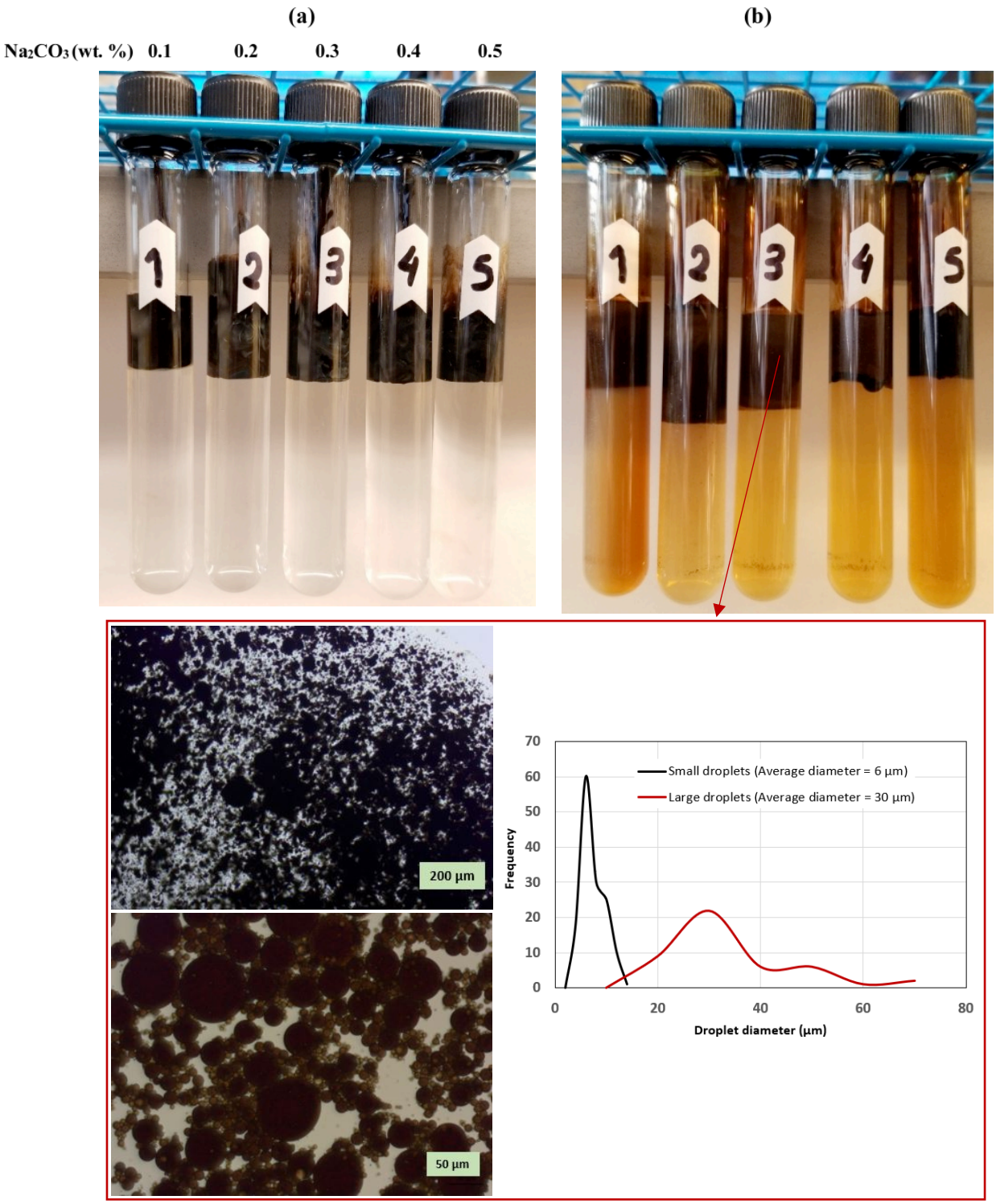

Fig. 5: WOR = 4 to 1 (4 gr aqueous phase + 1 gr heavy oil) a) before rotating b) 24 days after rotating at equilibrium state (anionic surfactant and polymer concentrations are constant in all the vials and equal to 0.1 wt. % (1,000 ppm)) (sodium carbonate concentration increased from 0.1 to 0.5 with 0.1 increments, as indicated above the vials in (a))

As shown in Fig. 5a, the interface between aqueous phases and heavy oil is flat due to the presence of 0.1 wt. % surfactant and increasing concentration of alkaline. In the absence of these chemicals, this interface is curved (see Fig. 3a, Arab *et al*., 2018). This lack of curvature indicates the effect of these chemicals to reduce IFT, as discussed later in this article. Increasing concentration of alkaline affects the type of emulsions: vial 1 contains type II (-), based on the Nelson and Pope (Nelson and Pope, 1978) definition, which is equivalent to Winsor type 1, based on the Winsor (Winsor, 1954) definition. This is an oil in water emulsion, as shown in bottom phase of vial 1 in Fig. 5b. The oil swelling observed in Vial 2 in Fig. 5b indicates formation of water in oil emulsion. In this case, there is oil creamed at the top separated with the middle phase emulsion from the bottom aqueous phase (vial 2 in Fig. 5b). This water in oil emulsion has a very high viscosity (21,000 mPa.s, obtained through measuring the viscosity of the middle phase from vial 2 in Fig. 5b), which may lead to potential injectivity problems in field applications. Vial 3 in Fig. 5b contains a type II (+) emulsion, based on the Nelson and Pope (Nelson and Pope, 1978) definition. In this case, the viscosity of the upper phase microemulsion is 740 mPa.s, which is 5 % of the originating oil with viscosity of 14,850 mPa.s. This enhanced viscous oil emulsification is not observed at higher concentrations of alkaline (see vial 4 and 5 in Fig. 5b). The microscopic images of the upper phase of vial 3 and the histogram of the droplet size distributions, obtained through applying *regionprops* module from scikit-image (an Open-Source image processing library), are enclosed in bottom part of Fig. 5. As shown, the emulsion droplets show a bimodal distribution with 6 and 30 μm as the two peaks with the largest frequencies of 60 and 22, respectively.

Viscosity measurements

Viscosity of SP solution (0.1 wt. % concentrations of each) with increasing concentration of Na_2CO_3 was measured (Fig. 6). As shown in Fig. 6, increasing alkaline concentration up to 0.4 wt. % only slightly affects the SP solution viscosity. The SP solution viscosity at 5 s^{-1} shear rate in the absence of Na_2CO_3 is 95.7 cP, which can be considered as an estimated viscosity of polymer alone solution assuming addition of only 0.1 wt. % of surfactant has negligible effect on viscosity. This value only slightly changes to 97.15 ± 7.5 cP in the presence of up to 0.4 wt. % Na_2CO_3 (Fig. 6). With a further increase in alkaline concentration, on the other hand, there is a significant reduction in SP viscosity (13.56 cP at 5 s^{-1} shear rate in the presence of 1.5 wt. % Na_2CO_3, Fig. 6). Increasing alkaline concentration results in increasing ionic strength and pH, each of which has a competing effect on polymer solution viscosity (Sheng, 2017). Increasing ionic strength (acts as if increasing

salinity) inversely affects the thickness of double layer which in turn, lowers the repulsion between polymer molecules. As a result, they tend to be coiled rather than being extended (Gbadamosi *et al*., 2019). On the other hand, increasing alkalinity enhances the degree of hydrolysis of polyacrylamide molecules, which converts amide groups ($CONH_2$) to carboxyl groups (COO^-), which in turn enhances thickening of the solution (Gbadamosi *et al*., 2019). However, it is widely reported that the effect of increasing ionic strength to reduce double layer repulsion between polymer molecules is more pronounced compared to the effect of increasing pH to enhance the degree of hydrolysis and so adding alkaline generally reduces polymer viscosity (Kang, 2001). Our observations suggest that adding low concentrations of alkaline, lower than 0.4 wt. %, does not affect the viscosity of SP solution (Fig. 6).

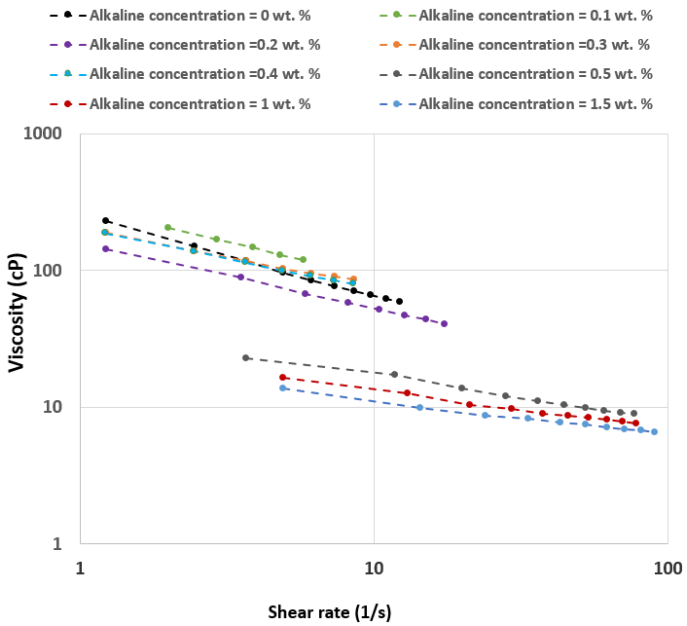

Fig. 6: (a) Viscosity of chemical formulations containing fixed concentrations of anionic surfactant (0.1 wt. %) and polymer (0.1 wt. %) with increasing concentration of sodium carbonate from 0 to 1.5, as indicated in the legends (b) zoomed into the plot to more clearly show the data for shear rates up to 20 s^{-1}

Interfacial tension measurements

The interfacial tension between heavy oil and an aqueous phase loaded with a fixed concentration of anionic surfactant (0.1 wt. %) and increasing concentrations of sodium carbonate is shown in Fig. 7. IFT could not be measured through spinning drop technique when there was a polymer in an aqueous phase. However, polymer molecules have been reported to have a minimal effect on

IFT (Sheng, 2017). As shown in Fig. 7, the ultralow IFT is achieved when sodium carbonate concentration is between 0.1 and 0.5 wt. %. This ultralow IFT is resulted from the effect of both synthetic surfactant and in-situ soap generated due to the reaction of acidic oil with alkaline. The IFT in the presence of only 0.1 wt. % synthetic surfactant is 42.6 mN/m, while only 0.1 wt. % sodium carbonate reduces IFT to 0.020 mN/m. The IFT in the presence of 0.1 wt. % synthetic surfactant and 0.1 wt. % sodium carbonate is 0.002 mN/m.

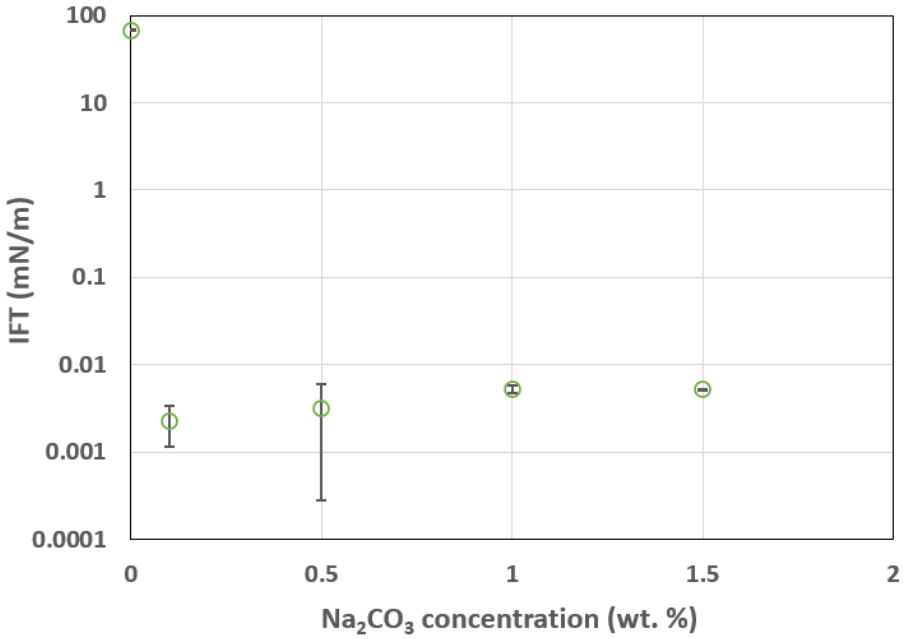

Fig. 7: Interfacial tension between heavy oil and an aqueous phase containing a fixed concentration of anionic surfactant (0.1 wt. %) with increasing concentration of sodium carbonate

Based on these screening experiments (batch mixing experiments, viscosity measurements, and IFT measurements), the combination of 0.1 wt. % synthetic anionic surfactant, 0.3 wt. % sodium carbonate, and 0.1 wt. The % polymer solution was selected for the following core flooding and microfluidic experiments.

Sand-pack core flooding experiments

Fig. 8 shows the results of the sand-pack core flooding experiments. Oil recovery to water injection for 7 PVI is 18 % OOIP, which is comparable in different runs. The pressure gradient was significantly increased to 32 psi/ft (723.9 KPa/m) in the secondary polymer flood accompanied

with 12 % OOIP incremental oil recovery. In the secondary ASP flood, although pressure gradient build-up is much less (8 psi/ft (180.9 Kpa/m) compared to the polymer flood, the incremental oil recovery is 18 %. In addition, the effluents of ASP flood are all low viscosity oil in water emulsions (see the vials' images enclosed in Fig. 8). These observations suggest sweep efficiency improvement should not be the primary mechanism contributing to viscous oil recovery. These observations are consistent with the results of batch mixing experiments presented in Fig. 5. The 15 % OOIP incremental oil was recovered in the extended water flood following the ASP flood. At around 9 PVI in the extended water flood after ASP flood, there is a pressure build-up to 15 psi/ft (339.3 KPa/m), which could be due to the plugging of the channels due to emulsions (Fig. 8). To visualize these speculations, three microfluidic experiments were designed. In these experiments, similar materials including the same viscous oil and chemicals, were used.

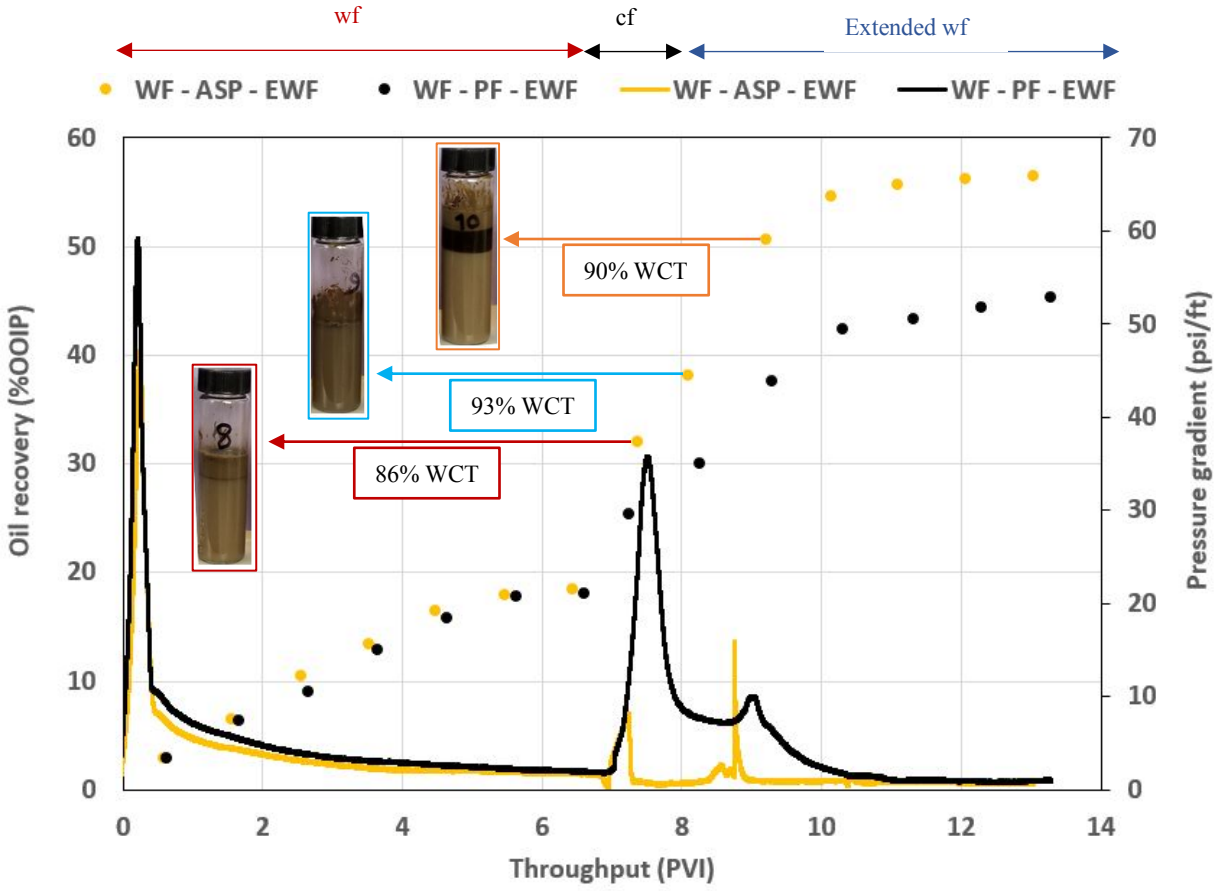

Fig. 8: Oil recovery (left y-axis) and pressure gradient across the core (right y-axis) as a function of PVI for sand-pack core flooding experiments

To quantify the force balance in different scenarios, residual oil saturation is plotted vs. normalized

capillary number, $\frac{K_{wor}C^*}{(M-1)\,K_{abs}/\phi}$ where M, C^*, K_{wor} and K_{abs}/ϕ are end point mobility ratio, a constant suggested as 306.25 for water-wet cores (Peters, 1979), end point permeability to water at residual oil saturation, and square of Leverett (Leverett, 1941) radius, respectively (Arab *et al.*, 2021). We previously showed that normalized capillary number could be well correlated to the practical residual oil saturation for a wide range of viscosity ratios in water-wet medium (Arab *et al.*, 2022). Based on our experimental conditions, we identified a critical normalized capillary number of 0.1, beyond which oil displacement in the water-wet medium is more pronounced (Arab *et al.*, 2022). The larger the normalized capillary number, the more stable flood with less severe viscous fingering, leading to more incremental oil recovery. This is the main reason behind the incremental oil recovery observed in slower floods (green data points in Fig. 9) compared to the high velocity floods (black data points in Fig. 9). The higher flood stability leading to larger oil recovery is achieved through thickening the injected water in polymer flood (red data point in Fig. 9) and enhanced emulsification in the ASP flood (orange data point in Fig. 9). These speculated mechanisms will be addressed in more detail through microfluidic experiments.

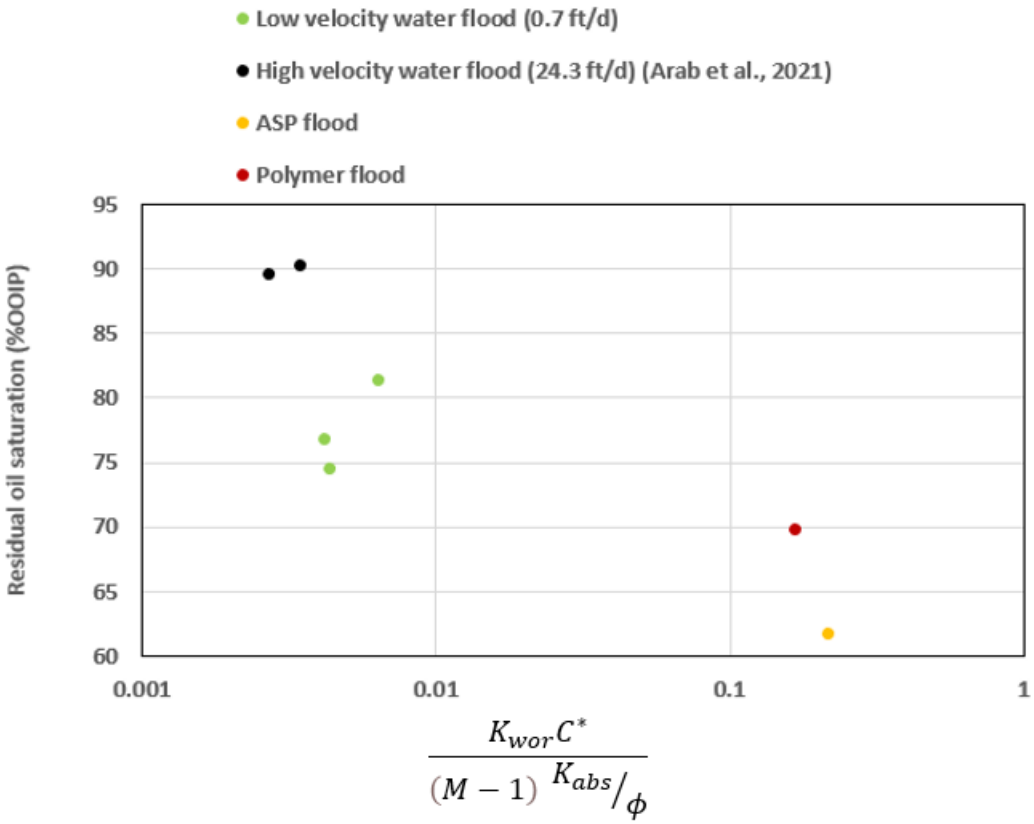

Fig. 9: Residual oil saturation vs. normalized capillary number

Microfluidic experiments

The results of the three experiments where chemical formulations were ASP, AS, and P are shown in Fig. 10, 11, and 14, respectively. All the other experimental settings applied in these experiments were the same.

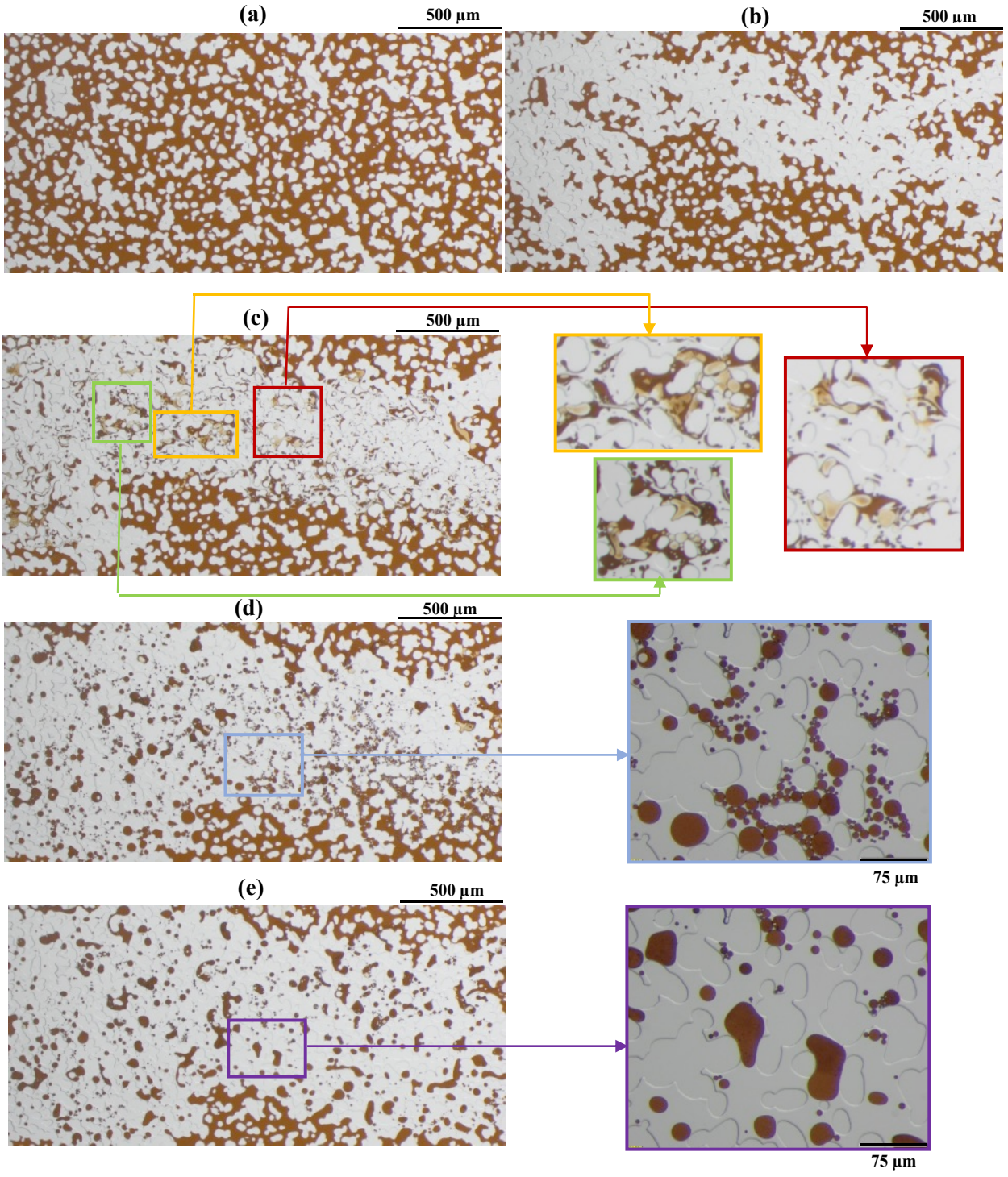

Fig. 10: ASP flood: a) initial condition at connate water saturation b) water flood c) ASP flood d) extended water flood conducted at the same velocity as the ASP flood e) extended water flood at high velocity (24.3 ft/d). In all images, brown represents oil, while water and grains are colorless.

The injected ASP efficiently emulsifies the residual ganglia, as shown in Fig. 10c. In this case, the low viscosity emulsions with droplet diameters (see Fig. 16d) smaller than the pore throats, depicted in the zoomed images enclosed in Fig. 10, are entrained. Also, the injected ASP was proved to efficiently entrain viscous oil from the edge of the main channel, which was left behind after the primary water flooding (Fig. 11). In the extended water flood, increasing viscous forces through increasing injection velocity facilitates the flow of oil in water emulsion droplets, as depicted in the magnified images of the same pore space flooded at different velocities (see Fig. 10d and 10e). In this case, the droplets of the double (water in oil in water) emulsions, depicted in Fig. 12, have been efficiently entrained in the extended water floods. These pore-scale observations explain the notable incremental oil recovery of 15 %OOIP observed in the extended water flood followed the ASP flood observed at the core scale (Fig. 8).

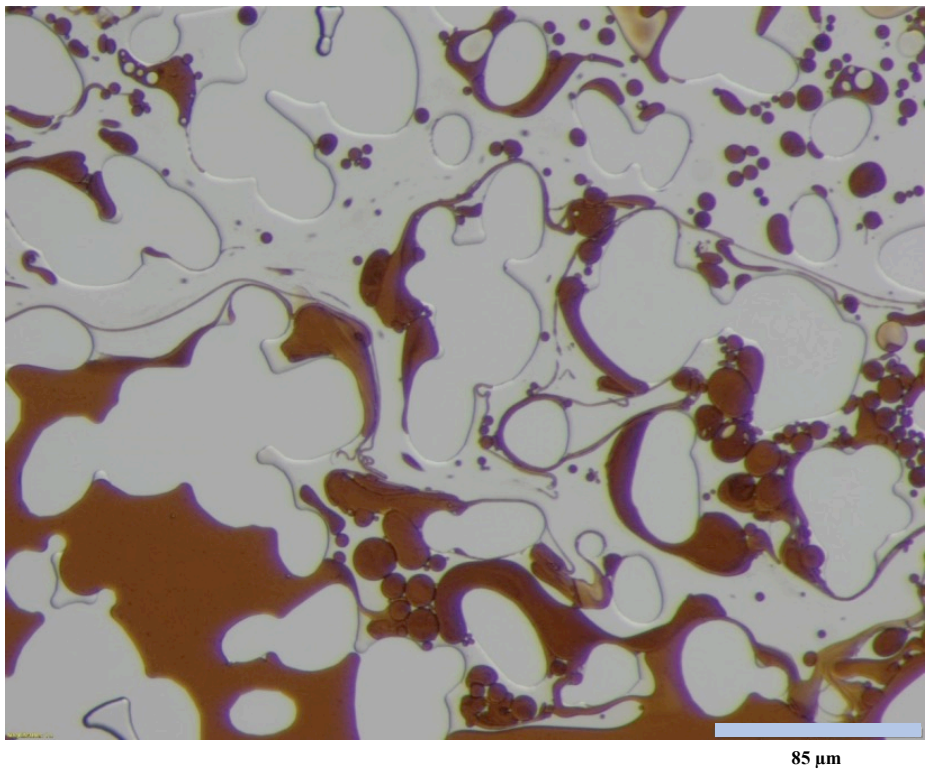

Fig. 11: Oil emulsification and stripping only observed in the ASP flood. In all images, brown represents oil, while water and grains are colorless.

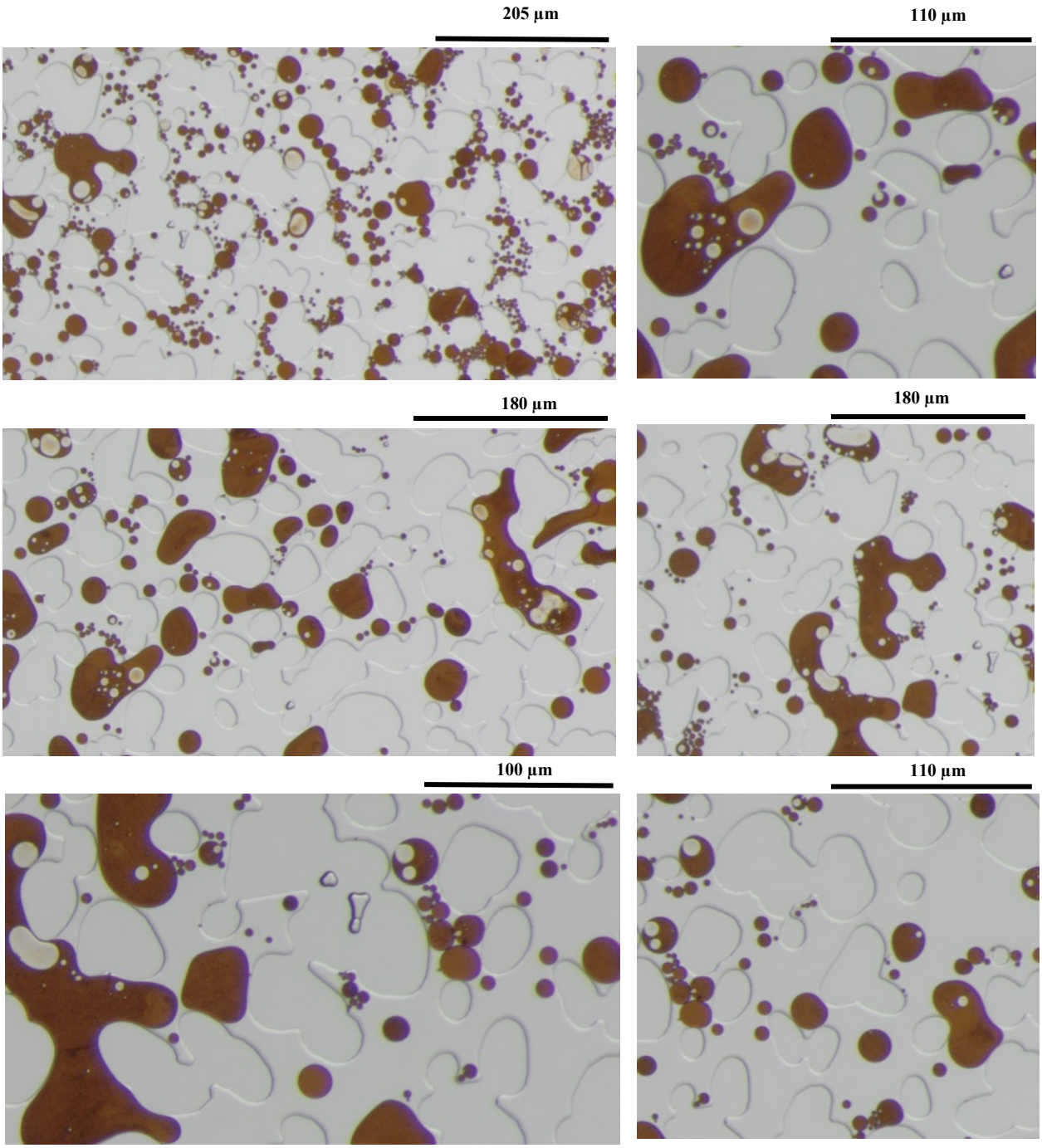

Fig. 12: Double (water in oil in water) emulsions observed in extended water flood post ASP. In all images, brown represents oil, while water and grains are colorless.

The significant emulsification observed due to the ASP flood was not observed in the AS flood. Given the same surfactant and alkaline concentrations as in the ASP flood, these observations emphasize the effect of polymer on emulsification. Comparing Fig. 10c and 13c reveals that

polymer is required to provide the sufficient driving force required for AS solution to contact the residual ganglia in the swept area or efficiently strip the oil from the channel edge. In the absence of polymer, the AS can slightly penetrate through the ganglia/channel leading to the small oil stripping from the edge (see the zoomed image enclosed in Fig. 13c). Therefore, the residual ganglia cannot be efficiently mobilized even after increasing the velocity in the extended water flood (see the ganglia depicted in the zoomed images enclosed in Fig. 13c and 13e). However, in the presence of polymer, the ASP can efficiently penetrate into the ganglia/channel's edge to enhance emulsification, making the process much more efficient than just stripping from the ganglia edge (see Fig. 10c, 10d and 10e). Although the presence of polymer is proved to play a critical role in ASP flood to mobilize oil, it is the least efficient chemical solution if applied alone. As shown in Fig. 14b, the injected polymer mainly circulates through the channel left behind in the preceding water flood with a very minuscule effect on oil recovery.

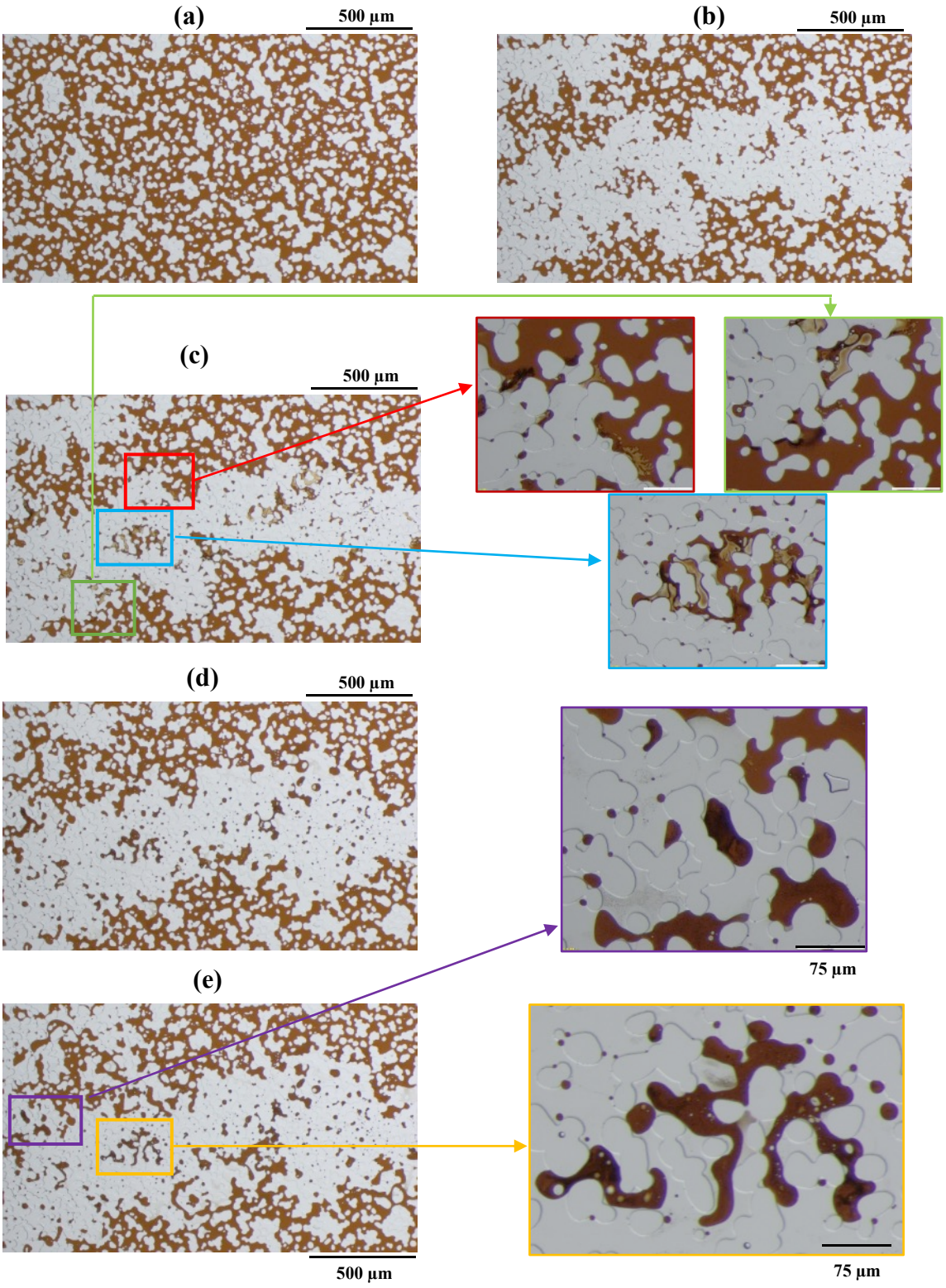

Fig. 13: AS flood: a) initial condition at connate water saturation b) water flood c) AS flood d) extended water flood conducted at the same velocity as the AS flood e) extended water flood at

high velocity (24.3 ft/d). In all images, brown represents oil while water and grains are colorless.

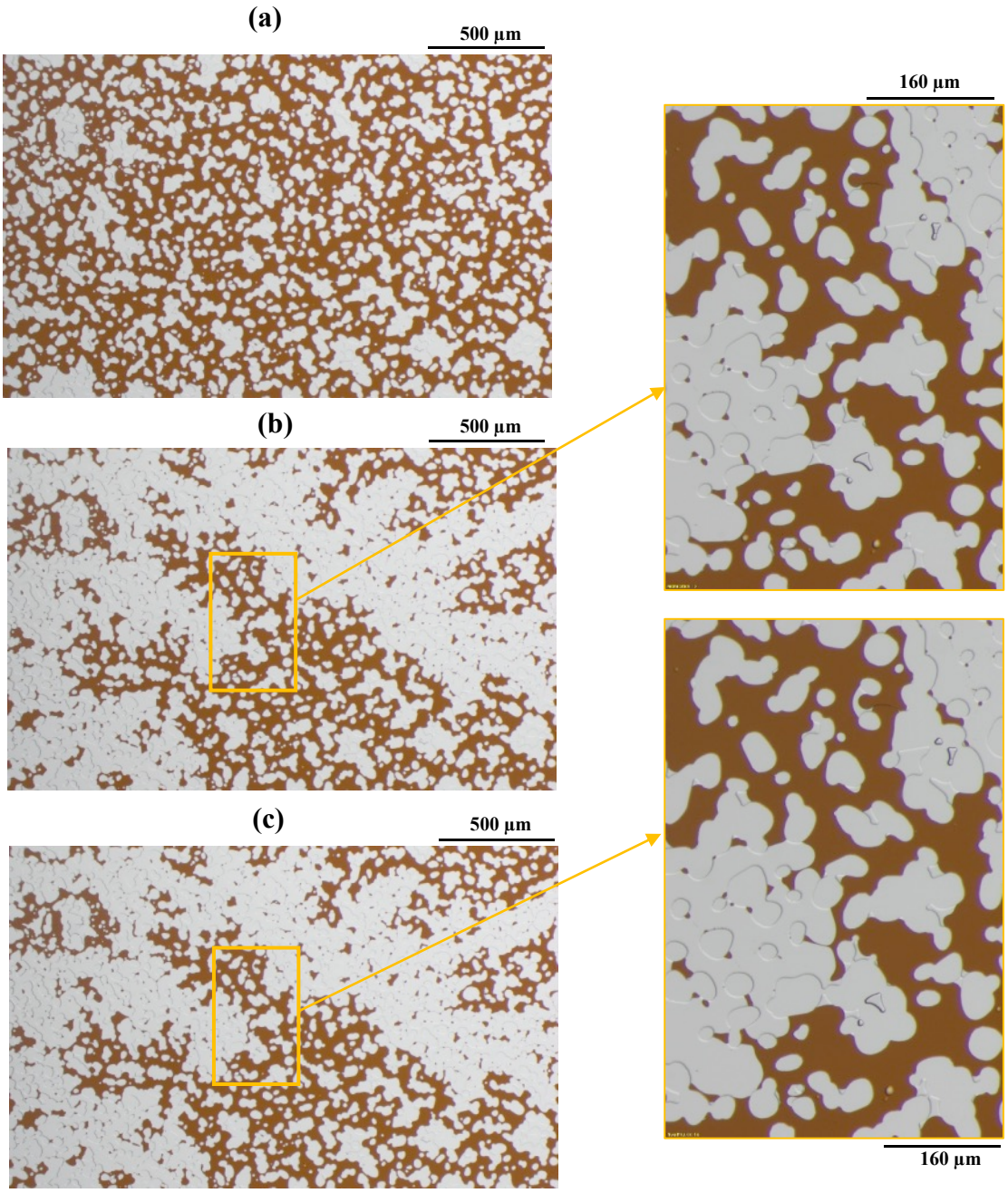

Fig. 14: P Flood: a) initial condition at connate water saturation b) water flood c) polymer flood. In all images, brown represents oil, while water and grains are colorless.

Oil recovery profiles, along with the corresponding number of oil clusters created during the floods, are presented in Fig. 15. The oil recovery to water injection after 5 PVI observed in different

runs is 37 ± 5 % OOIP (Fig. 11a). The variation in oil recovery to water flood in various runs can be attributed to the unstable flow and random formation of viscous fingers. This recovery to water flood is almost doubled compared to the oil recovery observed in the sand-pack flooding experiment (with a recovery of 18 %OOIP, see Fig. 8). This difference can be attributed to the much larger pore throat radius in the microfluidic chip (99 μm) compared to the sand-pack experiments with a pore throat radius estimated as 27 μm through the bundle of capillary tube model (Lake *et al.*, 2014). This difference may also be attributed to the fact that the microfluidic experiments simulate a 2-dimensional flow, whereas the sand-pack flooding experiments are considered 1-dimensional.

The results of the secondary chemical floods are presented in Fig. 15c and 15d. ASP injection leads to incremental oil recovery of 8 %OOIP. This is a result of the in-situ emulsification, quantified through the number of separated oil clusters (Fig. 15d). In this case, the number of oil clusters emulsified in the aqueous phase is significantly increased from 200, left at the end of primary water flooding, to 1200 at the end of ASP flood. These oil clusters with an average diameter of around 9 μm (see Fig. 16d) can be easily entrained through the pore throats leading to the observed incremental oil recovery. In the other extreme case, when the chemical contains only polymer solution, the number of oil clusters remains almost the same (around 400, see Fig. 15d), justifying no observed incremental oil recovery. Oil recovery profiles to the extended water floods following the secondary chemical floods are depicted in Fig. 15e. In these cases, there is no incremental oil recovery to the extended water injection following either P or AS injection. However, there is a 4 % OOIP incremental oil recovery to the extended water flood following the ASP injection. In this case, the number of oil clusters remains almost the same, see Fig. 15f, because the injected fluid is just water with no further in-situ emulsification. In this case, injected water only pushes the emulsion droplets already generated in the preceding ASP flood. Oil recovery to the high velocity (24.3 ft/d (8.57×10^{-5} m/s)) extended water floods are shown in Fig. 15g. In these experiments, there was a minuscule oil recovery when the chemical agent was only a polymer solution. However, there are 3 % OOIP and 6 % OOIP incremental oil recoveries to the high velocity extended water flood following AS, and ASP injection, respectively. In these cases, the number of oil clusters remains almost the same in the extended water flood following the AS injection, while it is remarkably reduced from 1300 to 860 in the extended water flood following the ASP injection (see Fig. 15h). In the latter case, the increasing viscous forces exerted through

increasing water injection velocity facilitates displacement of the generated emulsion droplets all the way to the production end, leading to a significant reduction in the number of oil clusters. To quantify these observations, some future microfluidic experiments with recording pressure gradient across the chip are required to investigate how well the data can be correlated with the normalized capillary number.

(a)

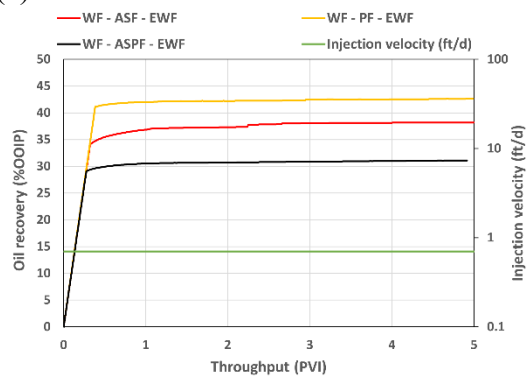

(b)

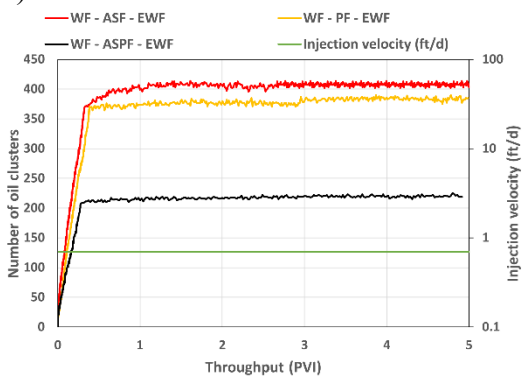

(c)

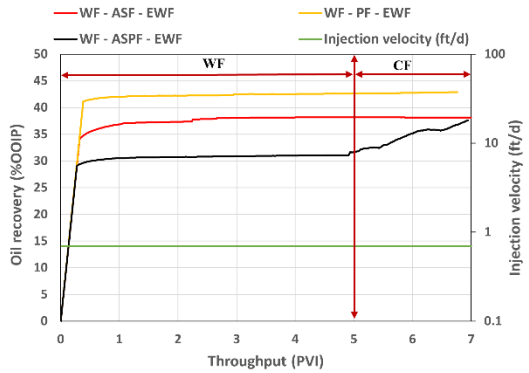

(d)

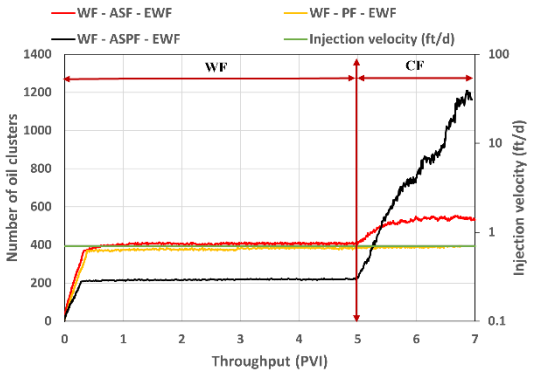

(e)

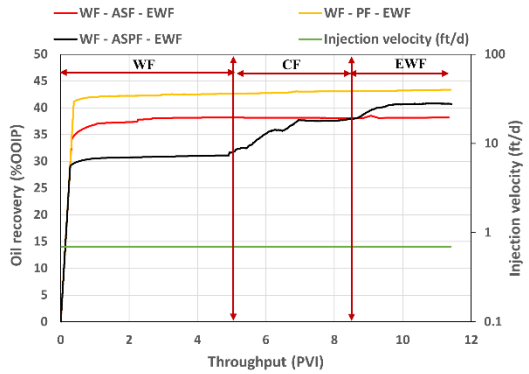

(f)

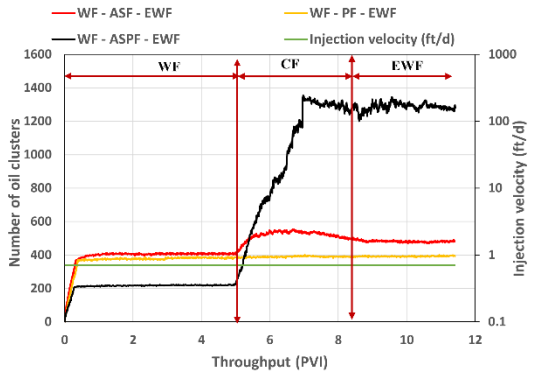

(g)

(h)

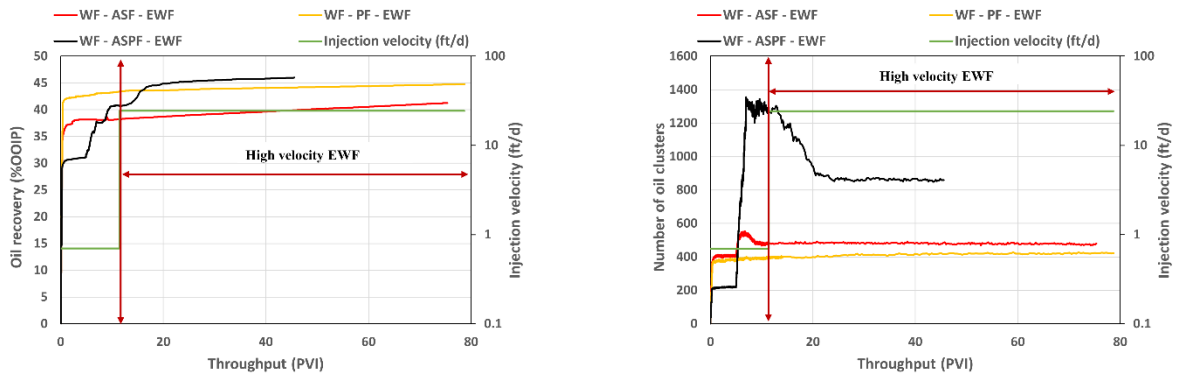

Fig. 15: Oil recovery profiles and the corresponding plots for the number of oil clusters created in different runs: a and b) water floods, c and d) secondary chemical floods, e and f) extended water floods at the same velocity (0.7 ft/d) as the preceding chemical floods, g and h) high velocity (24.3 ft/d (8.57×10^{-5} m/s)) extended water floods.

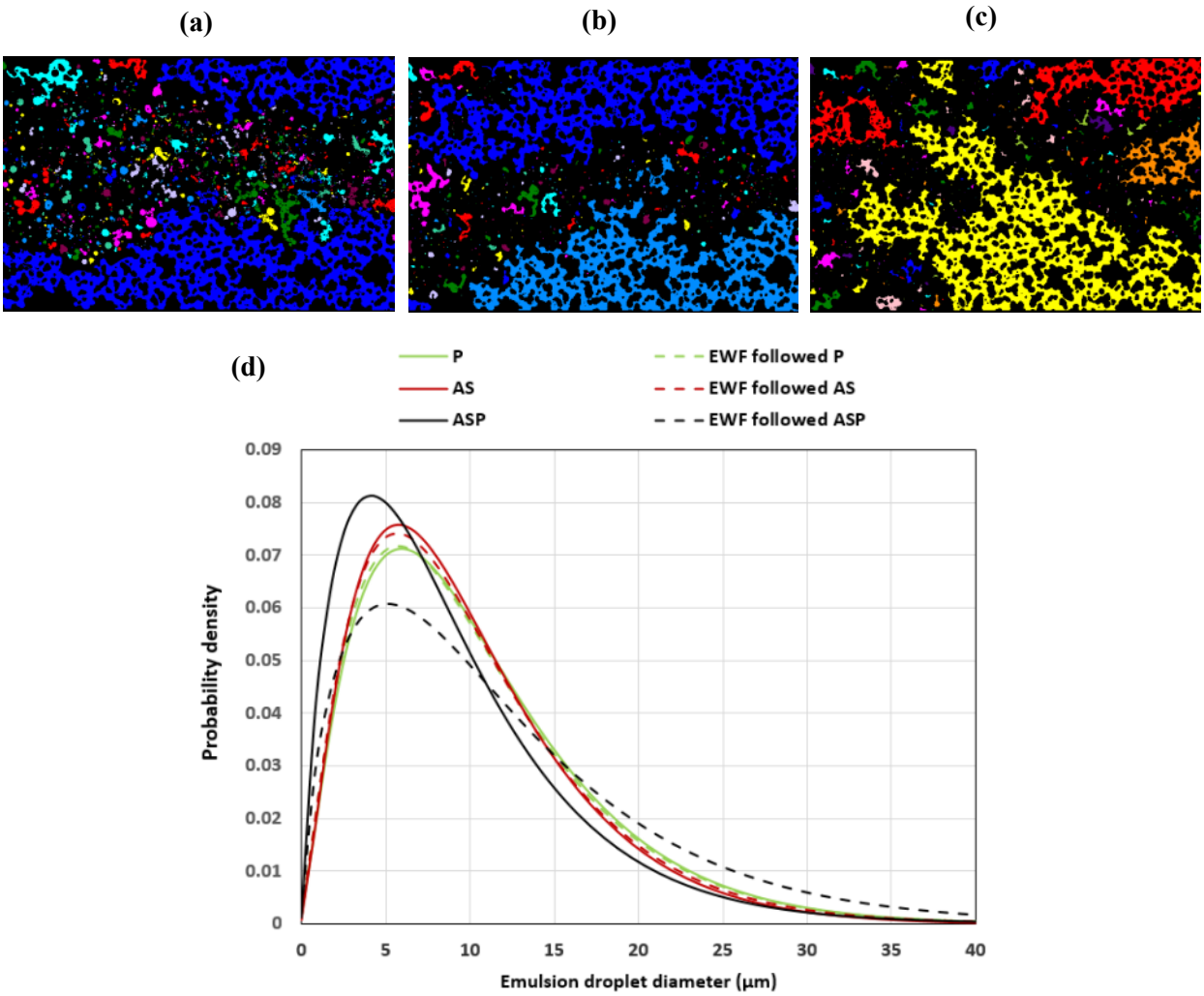

Fig. 16: a, b, and c are the labelled images corresponding to the images presented in Fig. 10d

(ASP flood), 13d (AS flood), and 14c (P flood), d) probability density function of the emulsion droplets labelled in a, b, and c (the probability density function of the emulsion droplets left at the end of the high-velocity water floods are also included in Fig. 16d, the corresponding labelled images are not shown)

To quantify the size of oil clusters created due to various chemicals, labelled images corresponding to the images presented in Fig. 10d (ASP flood), 13d (AS flood), and 14c (P flood) are shown in Fig. 16a, b, and c, respectively. In these images, each separated oil cluster is labeled through a different color, whose equivalent diameter was calculated through the *regionprops* module from the scikit-image library. The continuous untouched oil, left behind after the water breakthrough (shown in blue in Fig. 16a), is stripped due to the effect of ASP injection, which in turn widens the finger. This is also observed, to a smaller extent, in AS injection (Fig. 16b). This is insignificant when the injection solution is only polymer (Fig. 16c). These images were used to calculate the probability density function of oil clusters (Fig. 16d). The size distribution datasets were fitted to the Gamma distribution function (Fig. 16d): the average diameter of emulsion droplets in ASP flood is around 9 μm. These results are comparable with the droplet size analysis of the batch mixing experiments, shown in Fig. 5. The probability density function of oil clusters' diameter at the end of the experiments, i.e., at the end of high velocity extended water flooding, is also included in Fig. 16d (see the dashed lines). As shown, the distributions of oil clusters at the end of AS and P floods are comparable to those observed at the end of the high velocity extended water floods.

On the other hand, there is a significant reduction in the number of oil clusters due to the extended water injection following the ASP flood. As discussed, in this case, the chemical formulation efficiently emulsifies the oil in place with small sizes (around 9 μm on average), which can be pushed through the pore throats. This is the main reason behind the 6 % OOIP incremental oil recovery observed in the extended water flood following the ASP flood (see Fig. 15g).

Conclusions

Experiments including interfacial tension measurements, batch mixing tests, and viscosity measurements were applied to screen the most efficient chemical formulation to generate low viscosity type II (+) emulsion. To verify the effect of chemicals on viscous oil emulsification during fluid flow in porous media, core flooding experiments and pore-scale microfluidic tests were designed. Core flooding results show that the efficiently designed ASP cocktail can enhance

oil recovery (20% OOIP). This is almost twice the polymer injection that produces around 4.5 times larger pressure gradient across the core. This could be of great interest in field applications where oil recovery is desired while injectivity problems should be avoided. The normalized capillary number concept was used to explain the core scale observations. The efficiently designed ASP cocktail significantly improves flood stability with less viscous fingering, leading to the observed incremental oil recovery. The more stable flood provides more residence time for the oil in place to be exposed to the chemicals, enhancing emulsification. Based on the results of microfluidic experiments, the polymer component is essential in the efficiency of ASP flood. In the absence of polymer but with the same AS concentrations, the AS solution can slightly penetrate the untouched ganglia or the channels' edges from which oil stripping is minuscule. The oil stripping and emulsification of viscous oil were quantified through analysis of the labelled images obtained in different runs of microfluidic experiments. The average diameter of emulsion droplets created in the ASP injection in the microfluidic experiment is around 9 μm, which is comparable to what was observed in the batch mixing experiments.

Acknowledgement

This research was undertaken, in part, thanks to funding from the Canada Excellence Research Chairs Program. The authors gratefully acknowledge the financial support of the FUR program from NSERC, AITF, and the sponsoring companies: Athabasca Oil Corporation, Devon Canada (now CNRL), Foundation CMG (now Energi Simulation), Husky Energy (now Cenovus), Brion Energy (now Petro China Canada), Canadian Natural, Suncor Energy, ConocoPhillips, Enerplus and Chevron Canada, as well as the Schulich School of Engineering (University of Calgary). Danial Arab acknowledges with thanks support in the form of a Mitacs Accelerate Industrial Postdoctoral Program and Mitacs Globalink Research Award for partial funding of the project and employees of Porelab - Norwegian University of Science and Technology (NTNU) in Trondheim: Dr. Marie-Laure Olivier, Salem Akarri, and Roger Overå.

References

Aminzadeh, B., Hoang, V., Inouye, A., Izgec, O., Walker, D., Chung, D., Dwarakanath, V. (2016). Improving Recovery of a Viscous Oil Using Optimized Emulsion Viscosity. SPE-179698 presented at the SPE Improved Oil Recovery Conference, Tulsa, OK, April 11-13.

Arab, D., Kantzas, A., Bryant, S. L. (2018). Nanoparticle-Fortified Emulsification of Heavy Oil.

SPE-190377-MS presented at the SPE EOR Conference at Oil and Gas West Asia, Muscat, Oman, March 26-28.

Afrapoli, M. S., Alipour, S., Torsaeter, O. (2012). Analysis of microscopic displacement mechanisms of a MIOR process in porous media with different wettability. *Transport in porous media*, **93** (3), 705-719.

Anbari, A., Chien, H. T., Datta, S. S., Deng, W., Weitz, D. A., Fan, J. (2018). Microfluidic model porous media: Fabrication and applications. *Small*, **14** (18), 1703575.

Arab, D., Kantzas, A., Bryant, S. L. (2020). Water flooding of oil reservoirs: Effect of oil viscosity and injection velocity on the interplay between capillary and viscous forces. *Journal of Petroleum Science and Engineering*, **186**, 106691.

Arab, D., Bryant, S. L., Torsæter, O., Kantzas, A. (2022). Water flooding of sandstone oil reservoirs: Underlying mechanisms in imbibition vs. drainage displacement. *Journal of Petroleum Science and Engineering*, **213**, 110379.

Arab, D., Kantzas, A., Torsæter, O., Akarri, S., Bryant, S. L. (2021). A Crucial Role of the Applied Capillary Pressure in Drainage Displacement. *SPE Journal*, 1-19.

Banerjee, R., Kumar, S. J., Mehendale, N., Sevda, S., Garlapati, V. K. (2019). Intervention of microfluidics in biofuel and bioenergy sectors: technological considerations and future prospects. *Renewable and Sustainable Energy Reviews*, **101**, 548-558.

Bazazi, P., Sanati-Nezhad, A., & Hejazi, S. H. (2019). Role of chemical additives on water-based heavy oil mobilization: A microfluidic approach. *Fuel*, **241**, 1195-1202.

Bryan, J., Kantzas, A. (2008). Improved recovery potential in mature heavy oil fields by alkali-surfactant flooding. SPE-117649-MS presented at the International Thermal Operations and Heavy Oil Symposium, Calgary, Alberta, Canada, October 20-23.

Bryan, J., Kantzas, A. (2007). Enhanced Heavy-Oil Recovery by Alkali-Surfactant Flooding. SPE 110738 presented at the SPE Annual Technical Conference and Exhibition held in Anaheim, California, 11-14 Nov.

Chatenever, A., Calhoun, J. C. (1952). Visual examinations of fluid behavior in porous media-part I. *Journal of Petroleum Technology*, **4**(06), 149-156.

Chen, J.-D., and D. Wilkinson (1985). Pore-scale viscous fi ngering in porous media. *Phys. Rev. Lett*. **55**,1892–1895.

Dong, M., Ma, S., Liu, Q. (2009). Enhanced heavy oil recovery through interfacial instability: a

study of chemical flooding for Brintnell heavy oil. *Fuel*, **88** (6), 1049-1056.

Dong, M., Ma, S., Li, A. (2011). Sweep efficiency improvement by alkaline flooding for pelican lake heavy oil. GSUG/SPE 148971 presented at the Canadian Unconventional Resources Conference, Calgary, Alberta, November 2011.

Dittrich, P. S., Manz, A. (2006). Lab-on-a-chip: microfluidics in drug discovery. *Nature reviews Drug discovery*, **5**(3), 210-218.

El-Ali, J., Sorger, P. K., & Jensen, K. F. (2006). Cells on chips. *Nature*, **442**(7101), 403-411.

Farouq Ali, S. M. (2006). Practical heavy oil recovery.

Hirasaki, G. J., Miller, C. A., Puerto, M. (2008). Recent Advances in Surfactant EOR. SPE 115386 presented at the SPE Annual Technical Conference and Exhibition, Denver, 21-24 September.

Gbadamosi, A. O., Junin, R., Manan, M. A., Yekeen, N., Augustine, A. (2019). Hybrid suspension of polymer and nanoparticles for enhanced oil recovery. *Polymer Bulletin*, **76** (12), 6193-6230.

Gong, H., Li, Y., Dong, M., Ma, S., Liu, W. (2016). Effect of wettability alteration on enhanced heavy oil recovery by alkaline flooding. *Colloids and Surfaces A: Physicochemical and Engineering Aspects*, **488**, 28-35.

Guerrero, F., Bryan, J. L., Kantzas, A. (2018, March). Heavy Oil Recovery Mechanisms by Surfactant, Polymer and SP in a Non-Linear System. SPE-189722-MS, presented at the SPE Canada Heavy Oil Technical Conference, Calgary, Alberta, Canada, March 13.

Holtze, C. (2013). Large-scale droplet production in microfluidic devices—an industrial perspective. *Journal of Physics D: Applied Physics*, **46** (11), 114008.

Hu, J., Zhang, G., Jiang, P., Ge, J., Pei, H., Wang, X. (2022). Study on the chemical structure characterization and emulsification-stripping of heavy oil. *Journal of Petroleum Science and Engineering*, 110592.

Karadimitriou, N. K., Hassanizadeh, S. M. (2012). A review of micromodels and their use in two-phase flow studies. *Vadose Zone Journal*, **11**(3).

Kang, W.-L.,2001. Study of Chemical Interactions and Drive Mechanisms in Daqing ASP Flooding. Petroleum Industry Press, Beijing, China.

Kjeang, E., Djilali, N., Sinton, D. (2009). Microfluidic fuel cells: A review. *Journal of Power Sources*, **186** (2), 353-369.

Kumlangdudsana, P., Dubas, S. T., & Dubas, L. (2007). Surface modification of microfluidic devices. *Journal of Metals, Materials and Minerals*, **17** (2).

Kumar, R., Dao, E., Mohanty, K. K. (2012). Heavy-Oil Recovery by In-Situ Emulsion Formation. *SPE Journal*, **17**, 326-334.

Kunstmann-Olsen, C., Hoyland, J. D., & Rubahn, H. G. (2012). Influence of geometry on hydrodynamic focusing and long-range fluid behavior in PDMS microfluidic chips. *Microfluidics and nanofluidics*, **12** (5), 795-803.

Lake, L. W., Johns, R., Rossen, B. (2014). Fundamentals of Enhanced Oil Recovery, second edition. Richardson, Texas, USA: Society of Petroleum Engineers.

Li, S., Hadia, N. J., Lau, H. C., Torsæter, O., Stubbs, L. P., Ng, Q. H. (2018, June). Silica nanoparticles suspension for enhanced oil recovery: Stability behavior and flow visualization. SPE-190802-MS, presented at the SPE Europec featured at 80th EAGE Conference and Exhibition, Copenhagen, Denmark, June.

Lifton, V. A. (2016). Microfluidics: an enabling screening technology for enhanced oil recovery (EOR). *Lab on a Chip*, **16** (10), 1777-1796.

Liu, Q., Dong, M., Ma, S., Tu, Y. (2007). Surfactant enhanced alkaline flooding for Western Canadian heavy oil recovery. *Colloids and Surfaces A: Physicochemical and Engineering Aspects*, **293** (1), 63-71.

Liu, J., Qiao, H., Liu, C., Xu, Z., Li, Y., Wang, L. (2009). Plasma assisted thermal bonding for PMMA microfluidic chips with integrated metal microelectrodes. *Sensors and Actuators B: Chemical*, **141** (2), 646-651.

Liu, S., Miller, C. A., Li, R. F., Hirasaki, G. (2010). Alkaline/surfactant/polymer processes: wide range of conditions for good recovery. *SPE Journal*, **15** (02), 282-293.

Manrique, E. J., Muci, V. E., Gurfinkel, M. E. (2007). EOR field experiences in carbonate reservoirs in the United States. *SPE Reservoir Evaluation & Engineering*, **10** (06), 667-686.

Mei, S., Bryan, J., Kantzas, A. (2012). Experimental study of the mechanisms in heavy oil waterflooding using etched glass micromodel, SPE-157998-MS, presented at the SPE Heavy Oil Conference, Calgary, Alberta, Canada, June 12-14.

Mejia, L., Tagavifar, M., Xu, K., Mejia, M., Du, Y., Balhoff, M. (2019). Surfactant flooding in oil-wet micromodels with high permeability fractures. *Fuel*, **241**, 1117-1128.

Micronit Microtechnology Product document (https://store.micronit.com/media/productattach/e/o/eor_information_2021.pdf)

Nelson, R. C., Pope, G. A. (1978). Phase relationships in chemical flooding. *SPE Journal*, **18** (05),

325-338.

Nelson, R. C., Lawson, J. B., Thigpen, D. R., Stegemeier, G. L. (1984). Cosurfactant-enhanced alkaline flooding. SPE/DOE 12672 presented at the SPE Enhanced Oil Recovery Symposium. Tulsa, OK, April 15-18.

Neethirajan, S., Kobayashi, I., Nakajima, M., Wu, D., Nandagopal, S., Lin, F. (2011). Microfluidics for food, agriculture and biosystems industries. *Lab on a Chip*, **11** (9), 1574-1586.

Ott, H., Kharrat, A., Borji, M., Clemens, T., Arnold, P. (2019). Screening of EOR potential on the pore scale by statistical and topological means. In The SOCIETY OF CORE ANALYSTS 2019.

OpenCV documentation on Gabor kernels, https://docs.opencv.org/3.4/d4/d86/group__imgproc__filter.html#gae84c92d248183bd92fa713ce51cc3599

Rangriz Shokri, A., Babadagli, T. (2016). A sensitivity analysis of cyclic solvent stimulation for Post-CHOPS EOR: application on an actual field case. *SPE Econ. Manag.* **8** (04), 78–89.

Riahi, R., Tamayol, A., Shaegh, S. A. M., Ghaemmaghami, A. M., Dokmeci, M. R., Khademhosseini, A. (2015). Microfluidics for advanced drug delivery systems. *Current Opinion in Chemical Engineering*, **7**, 101-112.

Sackmann, E. K., Fulton, A. L., & Beebe, D. J. (2014). The present and future role of microfluidics in biomedical research. *Nature*, **507**(7491), 181-189.

Sbragaglia, M., R. Benzi, L. Biferale, S. Succi, K. Sugiyama, and F. Toschi (2007). Generalized lattice Boltzmann method with multirange pseudopotential. *Phys. Rev. E* **75**, 026702.

Sedaghat, M., Mohammadzadeh, O., Kord, S., Chatzis, I. (2016). Heavy oil recovery using ASP flooding: A pore- level experimental study in fractured five- spot micromodels. *The Canadian Journal of Chemical Engineering*, 94(4), 779-791.

Seo, S., Mastiani, M., Mosavati, B., Peters, D. M., Mandin, P., Kim, M. (2018). Performance evaluation of environmentally benign nonionic biosurfactant for enhanced oil recovery. *Fuel*, **234**, 48-55.

Schroen, K., Bliznyuk, O., Muijlwijk, K., Sahin, S., Berton-Carabin, C. C. (2015). Microfluidic emulsification devices: from micrometer insights to large-scale food emulsion production. *Current Opinion in Food Science*, **3**, 33-40.

Sheng, J. J. (2017). Critical review of alkaline-polymer flooding. *Journal of Petroleum Exploration and Production Technology*, **7** (1), 147-153.

Sim, S. S. K., Wassmuth, F. R., Bai, J. J. (2014). Identification of Winsor Type III Micro-Emulsion for Chemical EOR of Heavy Oil. SPE-170018-MS presented at the SPE Heavy Oil Conference, Calgary, AB, June10-12.

Su, H., Zhou, F., Zheng, A., Wang, L., Wang, C., Yu, F., Li, J. (2022). Heavy Oil Recovery by Alkaline-Cosolvent-Polymer Flood: A Multiscale Research Using Micromodels and Computed Tomography Imaging. *SPE Journal*, 1-13.

Tsakiroglou, C.D., and D.G. Avraam. (2002). Fabrication of a new class of porous media models for visualization studies of multiphase flow processes. *J. Mater. Sci*. **37**, 353.

Tong, D., Yesiloz, G., Ren, C. L., Madhuranthakam, C. M. R. (2017). Controlled synthesis of poly (acrylamide-co-sodium acrylate) copolymer hydrogel microparticles in a droplet microfluidic device for enhanced properties. *Industrial & Engineering Chemistry Research*, **56** (51), 14972-14979.

Wouters, B., Schoenmakers, P. J., Eeltink, S. (2014). Design of a microfluidic chip for spatial three-dimensional liquid chromatography separations. In 18th International Conference on Miniaturized Systems for Chemistry and Life Sciences, μTAS 2014.

Weng, X., Neethirajan, S. (2017). Ensuring food safety: Quality monitoring using microfluidics. *Trends in food science & technology*, **65**, 10-22.

Winsor, P.A., Solvent Properties of Amphiphillic Compounds, Butterworth Scientific Publication, London, England, 1954.

Xu, W., Ok, J. T., Xiao, F., Neeves, K. B., Yin, X. (2014). Effect of pore geometry and interfacial tension on water-oil displacement efficiency in oil-wet microfluidic porous media analogs. *Physics of fluids*, **26** (9), 093102.

Xu, J. H., Li, S. W., Tan, J., Wang, Y. J., Luo, G. S. (2006). Preparation of highly monodisperse droplet in a T- junction microfluidic device. *AIChE journal*, **52** (9), 3005-3010.

Xu, K., Liang, T., Zhu, P., Qi, P., Lu, J., Huh, C., Balhoff, M. (2017). A 2.5-D glass micromodel for investigation of multi-phase flow in porous media. *Lab on a Chip*, **17** (4), 640-646.

Zhou, X., Zeng, F., Zhang, L. (2016). Improving steam-assisted gravity drainage performance in oil sands with a top water zone using polymer injection and the fishbone well pattern. *Fuel* **184**, 449–465.

Zhang, Y., Ozdemir, P. (2009). Microfluidic DNA amplification—A review. *Analytica chimica acta,* **638**(2), 115-125.

Zhao, C. X. (2013). Multiphase flow microfluidics for the production of single or multiple emulsions for drug delivery. *Advanced drug delivery reviews*, **65**(11-12), 1420-1446.